

TIME-SERIES PHOTOMETRY OF GLOBULAR CLUSTERS: M62 (NGC 6266),
THE MOST RR LYRAE-RICH GLOBULAR CLUSTER IN THE GALAXY?

R. CONTRERAS,^{1,2} M. CATELAN,² H. A. SMITH,³ B. J. PRITZL,⁴ J. BORISSOVA,⁵ C. A. KUEHN³

AJ, in press

ABSTRACT

We present new time-series CCD photometry, in the *B* and *V* bands, for the moderately metal-rich ($[Fe/H] \simeq -1.3$) Galactic globular cluster M62 (NGC 6266). The present dataset is the largest obtained so far for this cluster, and consists of 168 images per filter, obtained with the Warsaw 1.3m telescope at the Las Campanas Observatory (LCO) and the 1.3m telescope of the Cerro Tololo Inter-American Observatory (CTIO), in two separate runs over the time span of three months. The procedure adopted to detect the variable stars was the optimal image subtraction method (ISIS v2.2), as implemented by Alard. The photometry was performed using both ISIS and Stetson's DAOPHOT/ALLFRAME package. We have identified 245 variable stars in the cluster fields that have been analyzed so far, of which 179 are new discoveries. Of these variables, 133 are fundamental mode RR Lyrae stars (RRab), 76 are first overtone (RRc) pulsators, 4 are type II Cepheids, 25 are long-period variables (LPV), 1 is an eclipsing binary, and 6 are not yet well classified. Such a large number of RR Lyrae stars places M62 among the top two most RR Lyrae-rich (in the sense of total number of RR Lyrae stars present) globular clusters known in the Galaxy, second only to M3 (NGC 5272) with a total of 230 known RR Lyrae stars. Since this study covers most but not all of the cluster area, it is not unlikely that M62 is in fact the most RR Lyrae-rich globular cluster in the Galaxy. In like vein, thanks to the time coverage of our datasets, we were also able to detect the largest sample of LPV's known so far in a Galactic globular cluster.

We analyze a variety of Oosterhoff type indicators for the cluster, including mean periods, period distribution, Bailey diagrams, and Fourier decomposition parameters (as well as the physical parameters derived therefrom). All of these indicators clearly show that M62 is an Oosterhoff type I system. This is in good agreement with the moderately high metallicity of the cluster, in spite of its predominantly blue horizontal branch morphology – which is more typical of Oosterhoff type II systems. We thus conclude that metallicity plays a key role in defining Oosterhoff type. Finally, based on an application of the “A-method,” we conclude that the cluster RR Lyrae stars have a similar He abundance as M3, although more work on the temperatures of the M62 RR Lyrae is needed before this result can be conclusively established.

Subject headings: stars: horizontal-branch – stars: variables: other – Galaxy: globular clusters: individual (M62, NGC 6266)

1. INTRODUCTION

By the early 1990's, it was widely perceived that “most variable stars that belong to Galactic globular clusters have by now been discovered” (Suntzeff et al. 1991). Indeed, Suntzeff et al. estimated that only a few percent of the total population of RR Lyrae variable stars remained to be discovered in globular clusters. However, most of the pre-1990 studies based their results on photographic photometry, which in many cases appears not to have been precise enough to detect small-amplitude variables. On the other hand, new techniques, based on image subtraction algorithms, have been developed in the last years, which are capable of quickly, efficiently and automatically detecting star variations even in the most crowded fields (e.g., Alard 2000; Bramich 2008). In fact, several studies have reported substantial in-

creases in the reported globular cluster RR Lyrae populations using these techniques (e.g., Kaluzny, Olech, & Stanek 2001; Corwin et al. 2004; Zorotovic et al. 2009). It seems that, contrary to what was previously thought, the sample of RR Lyrae variables identified so far in Galactic globular clusters is significantly incomplete, thus rendering further analyses, based on high-quality CCD observations and image subtraction techniques, well worth the while.

NGC 6266 (M62) is a high-density ($\log \rho_c = 5.34 L_\odot \text{pc}^3$), highly reddened [$E(B-V) = 0.47$] cluster, and is also one of the most massive in our galaxy, with $M_V = -9.19$ (Harris 1996). Located at just 1.7 kpc from the Galactic center, it has also been classified as a possible post-core collapse globular cluster by Trager, Djorgovski, & King (1993, 1995) – a possibility which however was not confirmed by Beccari et al. (2006) in their study of the radial density profile of the cluster. Also worth mentioning is the fact that the cluster currently ranks fifth in the number of millisecond pulsars (Cocozza et al. 2008, and references therein).

The morphology of the cluster's horizontal branch (HB) shows a prominent blue component, in addition to a very extended blue tail, reaching down to at least the main sequence turnoff level (e.g., Caloi et al. 1987; Piotto et al. 2002). The cluster is also known to be rich in RR Lyrae variables (Clement et al. 2001, and references therein). These features are strikingly similar to those of M15 (NGC 7078), perhaps

¹ INAF-Osservatorio Astronomico di Bologna, via Ranzani 1, 40127, Bologna, Italy

² Pontificia Universidad Católica de Chile, Departamento de Astronomía y Astrofísica, Av. Vicuña Mackenna 4860, 782-0436 Macul, Santiago, Chile

³ Department of Physics and Astronomy, Michigan State University, East Lansing, MI 48824

⁴ Department of Physics and Astronomy, University of Wisconsin, Oshkosh, WI 54901

⁵ Departamento de Física y Astronomía, Facultad de Ciencias, Universidad de Valparaíso, Ave. Gran Bretaña 1111, Playa Ancha, Casilla 5030, Valparaíso, Chile

the best known Oosterhoff type II globular cluster. Yet, M62 is more metal-rich by about 1 dex, with an $[\text{Fe}/\text{H}] = -1.29$, compared with $[\text{Fe}/\text{H}] = -2.26$ for M15 (Harris 1996). Since there is significant debate as to whether metallicity or HB morphology play the dominant role in defining the Oosterhoff types of globular clusters (e.g., Clement 2000; Pritzl et al. 2002), M62 can provide a very important constraint on whether metallicity differences, at a fixed HB morphology, can by themselves change the classification of an object from Oosterhoff type II (as in the case of M15) to Oosterhoff type I (as is typical of globular clusters with metallicity similar to M62's, but with significantly redder HB types).

The main time-series study of M62 available in the literature so far was carried out by van Agt & Oosterhoff (1959), where extensive photographic observations were presented, and periods derived for a total of 74 (out of 83) stars. More recently, Malakhova et al. (1997) provided a list of 43 additional RR Lyrae star candidates in the cluster, but without determining their periods nor their detailed variability status. As a consequence, 126 variable star candidates have been listed for the cluster, 74 of which have known periods of variability (Clement et al. 2001, and references therein).

Given the availability of high-quality CCD observations

and state-of-the-art image subtraction techniques, we expected to find many new variable stars in the course of our new time-series study of M62. Indeed, we were able to find more than 200 RR Lyrae stars in M62, in addition to a large number of long-period variables (LPV's) and type II Cepheids (CpII).

As reported in Contreras et al. (2005), the newly detected RR Lyrae stars in M62 offer us important insight into the role played by metallicity in defining Oosterhoff type, suggesting that M62 is indeed an Oosterhoff type I (OoI) object, in spite of its predominantly blue HB morphology, but in accord with its fairly high metallicity.

The main purpose of the present paper is to provide the new, extensive variability data for M62, upon which the preliminary results by Contreras et al. (2005) were based. We begin in §2 by describing our data and reduction procedures. In §3 we discuss how the variable stars were detected in our data. In §4 we describe the results of a Fourier decomposition analysis of the measured light curves. A CMD is produced in §5, where our approach to account for the effects of differential reddening is also described. In §6 we revisit the Oosterhoff type determination for the cluster. In §7 we apply the “A-method” to study the He abundance in the cluster, and in §8 we provide a summary of our results.

Table 1
Photometric Parameters for M62 Variables

ID	RA (J2000)	DEC (J2000)	P (d)	A_B	A_V	$\langle B \rangle$	$\langle V \rangle$	$(B-V)_{\text{mag}}$	$E(B-V)$	Type
V1	255.317419	-30.113051	0.5047	RRab
V2	255.295900	-30.134135	10.59	1.164	1.054	14.408	13.418	1.036	...	CpII
V3	255.275491	-30.116931	0.4913	RRab
V4	255.273855	-30.126022	0.54113	1.382	1.068	16.889	16.109	0.820	0.511	RRab
V6	255.277571	-30.105578	0.4920	1.363	1.082	16.861	16.121	0.772	0.442	RRab
V7	255.310374	-30.068129	0.5640	1.235	0.946	16.799	16.044	0.785	0.462	RRab
V8	255.273122	-30.070173	0.5327	1.315	1.009	16.779	16.034	0.780	0.462	RRab
V10	255.157448	-30.071484	0.53259	1.531	1.208	16.616	15.948	0.710	0.387	RRab
V11	255.156348	-30.080112	0.59823	0.994	0.749	16.651	15.921	0.746	0.369	RRab
V13	255.302296	-30.105842	0.3033	RRc
V16	255.279503	-30.088975	0.594	1.441	1.105	16.620	15.883	0.774	0.434	RRab
V17	255.296272	-30.086534	0.529	1.475	1.135	16.873	16.109	0.803	0.480	RRab
V18	255.292820	-30.089474	0.5241	1.285	1.027	16.937	16.156	0.806	0.461	RRab
V19	255.298855	-30.096809	0.5227	RRab
V20	255.345754	-30.070601	0.47201	1.590	1.252	16.842	16.099	0.792	0.499	RRab
V21	255.337973	-30.092659	0.4502	1.651	1.301	16.990	16.267	0.781	0.497	RRab
V22	255.324073	-30.111547	0.5013	RRab
V23	255.280529	-30.125258	0.44821	0.693	0.306	16.011	14.699	1.329	...	RRab
V24	255.323323	-30.125505	0.5223	1.480	1.121	17.309	16.422	0.932	0.620	RRab
V25	255.353541	-30.134815	0.4459	1.691	1.292	17.463	16.626	0.890	0.596	RRab
V26	255.245931	-30.198522	0.3717	1.680	1.210	14.343	13.547	0.862	0.607	RRab
V27	255.302024	-30.131513	0.44916	1.703	1.382	17.183	16.361	0.869	0.562	RRab
V28	255.353523	-30.109435	0.4978	1.424	1.123	17.348	16.610	0.774	...	RRab
V29	255.353458	-30.110630	0.5653	1.551	1.184	17.238	16.396	0.888	0.574	RRab
V30	255.285077	-30.165287	0.3041	0.565	0.422	17.308	16.502	0.813	...	RRc
V31	255.289800	-30.154549	0.4855	1.577	1.271	17.496	16.590	0.954	0.655	RRab
V32	255.304371	-30.152469	0.5479	1.315	0.953	17.499	16.571	0.966	0.688	RRab
V33	255.300167	-30.147727	0.5736	1.273	0.973	17.600	16.620	1.009	0.688	RRab
V34	255.284474	-30.116560	0.5834	1.402	1.053	16.789	15.955	0.876	0.559	RRab
V35	255.267377	-30.108630	0.5292	1.271	0.975	16.942	16.153	0.822	0.499	RRab
V36	255.290154	-30.080264	0.6527	0.819	0.659	16.730	15.933	0.810	0.442	RRab
V37	255.286882	-30.113188	0.5844	RRab
V38	255.297099	-30.127381	0.77083	RRab
V39	255.264623	-30.098901	0.6401	0.607	0.479	16.897	16.065	0.840	0.470	RRab
V40	255.264299	-30.102617	0.3012	0.622	0.531	16.790	16.124	0.673	...	RRc
V41	255.265477	-30.103925	0.5590	1.078	0.801	16.909	16.112	0.821	0.482	RRab
V42	255.261784	-30.101339	0.2469	0.434	0.351	16.689	16.085	0.608	...	RRc
V43	255.285001	-30.171389	0.56356	1.159	0.859	17.377	16.481	0.925	0.832	RRab
V44	255.289436	-30.148943	0.4456	1.471	1.122	17.631	16.724	0.954	0.681	RRab
V45	255.324166	-30.166686	0.51688	RRab
V48	255.276867	-30.151301	0.7432	0.934	0.725	17.108	16.185	0.940	0.571	RRab
V49	255.349296	-30.143648	0.5434	1.239	0.962	17.414	16.524	0.918	0.599	RRab
V50	255.394967	-30.123945	0.50264	RRab
V51	255.398036	-30.060953	0.2618	0.617	...	16.883	RRc

Table 1 — *Continued*

ID	RA (J2000)	DEC (J2000)	P (d)	A_B	A_V	$\langle B \rangle$	$\langle V \rangle$	$(B-V)_{\text{mag}}$	$E(B-V)$	Type
V52	255.328949	-30.165131	0.50538	RRab
V53	255.268551	-30.143154	0.2731	0.654	0.502	17.296	16.512	0.794	...	RRc
V56	255.315460	-30.081934	0.5616	1.164	0.857	17.089	16.249	0.864	0.520	RRab
V57	255.319997	-30.081330	0.5564	1.096	0.854	17.074	16.235	0.864	0.535	RRab
V58	255.272245	-30.106241	0.481	1.159	0.996	16.832	RRab
V59	255.343055	-30.088719	0.5791	1.148	0.871	17.093	16.250	0.870	0.550	RRab
V61	255.372598	-30.061961	0.2660	0.655	...	17.095	RRc
V62	255.380443	-30.085530	0.54807	1.235	0.958	17.048	16.230	0.845	0.519	RRab
V63	255.338601	-30.143041	0.6421	0.831	0.612	17.533	16.547	1.001	0.642	RRab
V64	255.361610	-30.195524	0.47299	0.785	0.592	17.077	16.157	0.937	0.614	RRab
V65	255.275462	-30.077039	0.2523	0.485	0.397	16.705	16.086	0.623	...	RRc
V66	255.201993	-30.110297	0.33383	0.570	0.420	16.676	16.011	0.674	...	RRc
V69	255.343090	-30.084393	0.3136	0.556	0.417	16.996	16.249	0.754	...	RRc
V72	255.245694	-30.144019	0.468	1.422	1.053	17.034	16.286	0.795	0.529	RRab
V73	255.238968	-30.144283	1.70	1.036	0.788	16.147	15.243	0.923	...	CpII
V74	255.297471	-30.129784	0.4667	RRab
V77	255.392629	-30.105263	0.319	0.531	0.405	17.240	16.427	0.820	...	RRc
V78	255.412564	-30.066713	0.62170	0.880	0.613	17.326	16.362	0.979	0.619	RRab
V80	255.276084	-30.089919	0.5962	0.914	0.645	16.985	16.090	0.911	0.739	RRab
V81	255.267912	-30.088047	0.5309	1.325	1.042	16.821	16.078	0.774	0.449	RRab
V82	255.291579	-30.133857	0.5648	0.835	0.642	17.291	16.479	0.826	0.483	RRab
V83	255.309339	-30.120442	0.4676	RRab
NV84	255.271467	-30.134929	0.7312	0.636	0.461	17.003	16.111	0.900	0.523	RRab
NV85	255.276401	-30.139297	0.3196	0.484	0.432	17.189	16.365	0.826	...	RRc
NV86	255.282427	-30.095331	0.2913	0.565	0.433	16.795	16.112	0.690	...	RRc
NV87	255.284966	-30.088009	0.6424	0.401	0.296	16.876	16.049	0.830	0.449	RRab
NV88	255.285771	-30.091009	0.5807	0.922	0.737	16.924	16.129	0.810	0.437	RRab
NV89	255.288146	-30.130509	0.5581	RRab
NV90	255.290712	-30.138332	0.3273	0.602	0.462	17.391	16.534	0.865	...	RRc
NV91	255.293574	-30.132221	0.3167	0.521	0.421	17.090	16.337	0.758	...	RRc
NV92	255.294328	-30.135833	0.5256	RRab
NV93	255.298447	-30.097374	0.552	1.205	0.966	17.249	16.340	0.935	0.600	RRab
NV94	255.306828	-30.090652	0.3181	RRc
NV95	255.311633	-30.142402	0.4941	1.618	1.226	17.533	16.609	0.970	0.668	RRab
NV96	255.315438	-30.140551	0.4663	1.582	1.257	17.452	16.615	0.880	0.572	RRab
NV97	255.323047	-30.096211	0.5510	1.166	0.883	17.096	16.262	0.861	0.534	RRab
NV98	255.321234	-30.147140	0.5620	1.113	0.878	17.611	16.670	0.969	0.645	RRab
NV99	255.323772	-30.144410	0.6028	0.565	0.410	17.661	16.644	1.023	0.653	RRab
NV100	255.332677	-30.100980	0.2665	0.612	0.490	17.097	16.370	0.735	...	RRc
NV101	255.331020	-30.146758	0.3055	0.493	0.397	17.333	16.516	0.821	...	RRc
NV102	255.334042	-30.094895	0.6307	0.737	0.541	17.048	16.174	0.885	0.523	RRab
NV103	255.331861	-30.150089	0.4836	0.825	0.611	17.588	16.655	0.949	0.602	RRab
NV104	255.335589	-30.111854	0.6307	0.306	0.221	17.290	16.380	0.913	...	RRc?
NV105	255.337117	-30.101376	0.5205	1.517	1.162	17.181	16.351	0.871	0.565	RRab
NV106	255.342344	-30.102395	0.5037	1.504	1.153	17.175	16.359	0.857	0.549	RRab
NV107	255.342654	-30.121002	0.5728	0.898	0.680	17.472	16.541	0.947	0.593	RRab
NV108	255.343116	-30.112112	0.2988	0.539	0.442	17.238	16.468	0.774	...	RRc
NV109	255.348015	-30.124260	0.6078	1.015	0.700	17.464	16.525	0.959	0.602	RRab
NV110	255.353263	-30.116493	0.3354	0.584	0.417	17.320	16.483	0.844	...	RRc
NV111	255.264451	-30.188755	0.2494	0.462	0.311	17.012	16.317	0.701	...	RRc
NV112	255.191976	-30.186995	0.503	RRab
NV113	255.323088	-30.186512	0.478	1.632	1.221	17.226	16.404	0.873	0.578	RRab
NV114	255.427287	-30.178179	0.398	1.063	1.010	18.423	17.135	1.294	...	EB
NV115	255.349885	-30.176159	0.2690	0.671	0.519	17.276	16.529	0.757	...	RRc
NV116	255.356841	-30.175140	0.615	0.558	0.390	17.290	16.384	0.913	0.551	RRab
NV117	255.247513	-30.170192	0.321	0.236	...	17.246	RRc
NV118	255.353800	-30.166045	0.2987	0.558	0.455	17.221	16.468	0.760	...	RRc
NV119	255.312109	-30.163121	0.3191	0.525	0.397	17.552	16.678	0.880	...	RRc
NV120	255.413338	-30.160585	0.489	1.658	1.271	RRab
NV121	255.299162	-30.159912	0.2805	0.498	0.378	18.060	17.251	0.814	...	RRc
NV122	255.222519	-30.139789	0.373	0.116	...	16.845	RRc
NV123	255.222694	-30.138895	0.3043	0.535	0.439	16.990	16.262	0.733	...	RRc
NV124	255.287656	-30.127940	0.4855	1.539	1.115	16.817	RRab
NV125	255.292043	-30.127814	0.2737	RRc
NV126	255.310969	-30.127268	0.5133	RRab
NV127	255.288948	-30.127077	0.5328	1.677	1.307	16.676	15.942	0.792	0.502	RRab
NV128	255.328694	-30.127022	0.2504	0.538	0.359	17.519	16.692	0.836	...	RRc
NV129	255.311556	-30.126846	0.3292	RRc
NV130	255.299567	-30.125709	0.2613	RRc
NV131	255.327951	-30.125428	0.3132	0.538	0.431	17.371	16.530	0.848	...	RRc
NV132	255.300206	-30.124985	0.2842	0.764	0.628	16.919	16.189	0.741	...	RRc
NV133	255.303920	-30.124868	0.3156	0.565	0.479	16.988	16.190	0.802	...	RRc
NV134	255.304938	-30.124915	0.336	RRc
NV135	255.212612	-30.124641	0.593	0.924	0.698	17.099	16.263	0.853	0.504	RRab
NV136	255.313600	-30.124235	0.6258	1.160	0.878	17.105	16.227	0.904	0.553	RRab
NV137	255.300694	-30.123833	0.515	RRab
NV138	255.303221	-30.123809	0.6051	RRab

Table 1 — *Continued*

ID	RA (J2000)	DEC (J2000)	P (d)	A_B	A_V	$\langle B \rangle$	$\langle V \rangle$	$(B-V)_{\text{mag}}$	$E(B-V)$	Type
NV139	255.304235	-30.123830	0.5405	RRab
NV140	255.313693	-30.123622	0.3830	0.541	0.427	16.905	16.097	0.813	...	RRc
NV141	255.302897	-30.123377	0.2994	RRc
NV142	255.324870	-30.122729	0.2758	RRc
NV143	255.299682	-30.121951	0.2959	RRc
NV144	255.297520	-30.121835	0.6105	RRab
NV145	255.310817	-30.121214	0.5665	RRab
NV146	255.296802	-30.121044	0.4660	RRab
NV147	255.301092	-30.120878	0.3259	RRc
NV148	255.307127	-30.120699	0.5606	RRab
NV149	255.300972	-30.120147	0.319	RRc
NV150	255.290041	-30.119827	0.5480	0.910	0.686	17.001	16.159	0.862	0.538	RRab
NV151	255.294859	-30.119358	0.3153	RRc
NV152	255.321269	-30.119151	0.3032	RRc
NV153	255.266009	-30.118983	0.3129	0.596	0.462	16.807	16.109	0.706	...	RRc
NV154	255.290525	-30.118882	0.3151	RRc
NV155	255.304738	-30.118780	0.271	RRc
NV156	255.301102	-30.118553	0.577	RRab
NV157	255.307981	-30.118448	0.7195	RRab
NV158	255.300638	-30.118371	0.264	RRc
NV159	255.289372	-30.118087	0.3763	RRc
NV160	255.292290	-30.118020	0.5437	1.482	1.218	16.933	16.147	0.819	0.487	RRab
NV161	255.310399	-30.117484	0.5568	RRab
NV162	255.304420	-30.117429	0.6032	RRab
NV163	255.306762	-30.117204	0.5943	RRab
NV164	255.303820	-30.116505	7.6	CpII
NV165	255.302432	-30.116402	0.4520	RRab
NV166	255.304920	-30.116240	0.290	RRc
NV167	255.314500	-30.116126	0.630	RRab
NV168	255.270280	-30.115961	0.5754	0.538	0.417	16.965	16.143	0.827	0.489	RRab
NV169	255.291652	-30.115633	0.5144	RRab
NV170	255.306553	-30.115631	0.635	?
NV171	255.318789	-30.115528	0.6482	0.322	0.254	17.159	16.246	0.914	...	RRc?
NV172	255.308393	-30.115490	0.3132	RRc
NV173	255.305549	-30.115363	0.347	RRc
NV174	255.301761	-30.115313	0.3175	RRc
NV175	255.321256	-30.115305	0.2816	0.643	0.516	17.08	16.372	0.725	...	RRc
NV176	255.305474	-30.114681	0.2628	RRc
NV177	255.291754	-30.114502	0.6851	RRab
NV178	255.304743	-30.114507	0.407	RRc
NV179	255.301488	-30.114427	0.5483	RRab
NV180	255.296731	-30.114401	1.376	CpII
NV181	255.295084	-30.113733	0.5895	RRab
NV182	255.300463	-30.113602	0.505	RRab
NV183	255.305893	-30.113635	0.5686	RRab
NV184	255.302188	-30.113549	0.5722	RRab
NV185	255.313926	-30.113517	0.591	RRab
NV186	255.307716	-30.113428	0.3025	RRc
NV187	255.298718	-30.113290	0.491	RRab
NV188	255.303150	-30.113177	0.436	RRab
NV189	255.315829	-30.113097	0.5617	RRab
NV190	255.302756	-30.112618	0.554	RRab
NV191	255.305548	-30.112558	0.5857	RRab
NV192	255.353057	-30.112569	0.2652	0.406	0.314	17.250	16.510	0.743	...	RRc
NV193	255.314500	-30.112496	0.3198	RRc
NV194	255.317154	-30.112403	0.505	RRab
NV195	255.298155	-30.112409	0.47	RRc
NV196	255.288121	-30.112265	0.3109	RRc
NV197	255.304747	-30.111837	0.3183	RRc
NV198	255.289817	-30.111245	0.5763	1.102	0.782	16.922	16.059	0.889	0.559	RRab
NV199	255.315134	-30.110762	0.5568	RRab
NV200	255.293965	-30.110272	0.487	RRab
NV201	255.314913	-30.108397	0.2507	RRc
NV202	255.307417	-30.108318	0.2709	0.517	0.439	16.974	16.258	0.720	...	RRc
NV203	255.301002	-30.108253	0.491	RRab
NV204	255.284814	-30.108090	0.263	0.415	0.329	16.922	16.224	0.701	...	RRc
NV205	255.295998	-30.107995	0.552	RRab
NV206	255.300336	-30.107351	0.640	RRab
NV207	255.299857	-30.106901	0.265	RRc
NV208	255.298778	-30.106808	0.5410	RRab
NV209	255.307591	-30.106368	0.2883	RRc
NV210	255.309869	-30.106245	0.4370	1.902	1.647	17.015	16.207	0.861	0.553	RRab
NV211	255.319518	-30.106219	0.3327	RRc
NV212	255.314221	-30.105641	0.6072	RRab
NV213	255.303032	-30.104438	0.5853	RRab
NV214	255.318374	-30.103102	0.587	1.004	0.776	17.154	16.299	0.875	0.538	RRab
NV215	255.305126	-30.102857	0.4616	RRab?

Table 1 — *Continued*

ID	RA (J2000)	DEC (J2000)	P (d)	A_B	A_V	$\langle B \rangle$	$\langle V \rangle$	$(B-V)_{\text{mag}}$	$E(B-V)$	Type
NV216	255.298332	-30.102701	0.2666	RRc
NV217	255.283447	-30.102377	0.3203	RRc
NV218	255.307103	-30.101639	0.4447	1.485	1.249	16.867	16.095	0.804	0.492	RRab
NV219	255.290591	-30.101456	0.7177	0.862	0.744	16.940	16.032	0.916	0.509	RRab
NV220	255.303126	-30.101010	0.496	RRab
NV221	255.265266	-30.091025	0.3300	0.555	0.425	16.802	16.085	0.725	...	RRc
NV222	255.250721	-30.080969	0.460	RRab
NV223	255.323255	-30.080828	0.5325	1.346	1.026	17.123	16.305	0.852	0.529	RRab
NV224	255.395528	-30.079961	0.3196	0.546	0.417	17.725	16.952	0.779	...	RRc
NV225	255.322496	-30.079209	0.2884	0.396	0.252	16.352	15.353	1.004	...	RRc
NV226	255.285658	-30.071786	0.6301	1.073	0.796	16.736	15.984	0.776	0.450	RRab
NV227	255.450562	-30.068877	0.456	1.725	1.290	18.629	17.774	0.899	0.564	RRab
NV228	255.334192	-30.068270	0.6417	0.380	0.322	17.132	16.253	0.881	0.479	RRab
NV229	255.337618	-30.066281	0.2773	0.295	0.248	16.765	16.106	0.660	...	RRc
NV230	255.332977	-30.096293	LP
NV231	255.324541	-30.097949	~16	LP/CpII?
NV232	255.321150	-30.136159	LP
NV233	255.318726	-30.108153	~49	LP
NV234	255.308946	-30.113105	LP
NV235	255.307303	-30.111160	LP
NV236	255.307158	-30.110023	~50	LP
NV237	255.303834	-30.130456	LP
NV238	255.304566	-30.106671	LP
NV239	255.303782	-30.113794	~75	LP
NV240	255.303710	-30.118210	LP
NV241	255.303521	-30.116544	0.525	RRab?
NV242	255.302059	-30.108011	~36	LP
NV243	255.301054	-30.113012	0.4911	RRab
NV244	255.298619	-30.119052	LP
NV245	255.297277	-30.084141	~88	LP
NV246	255.295958	-30.105957	0.5086	RRab
NV247	255.295155	-30.120411	0.4928	RRab
NV248	255.294099	-30.114300	LP
NV249	255.292809	-30.111699	0.2476	RRc
NV250	255.292034	-30.119580	~65	LP
NV251	255.290391	-30.115419	LP
NV252	255.281460	-30.119274	LP
NV253	255.280065	-30.102644	LP
NV254	255.278510	-30.126721	~90	LP
NV255	255.278235	-30.114604	LP
NV256	255.278240	-30.102156	LP
NV257	255.274444	-30.135636	~33	LP
NV258	255.308126	-30.120434	LP
NV259	255.298877	-30.063971	0.6704	RRab?
NV260	255.305121	-30.102731	0.2540	RRc
NV261	255.300681	-30.123291	0.5041	RRab
NV262	255.261271	-30.109493	LP

2. OBSERVATIONS AND DATA REDUCTIONS

M62 was observed in conjunction with M69 (NGC 6637; Escobar et al. 2010, in preparation) and NGC 5286 (Zorotovic et al. 2009, 2010) as part of a long-term project aimed at completing the census of (bright) variable stars in Galactic globular clusters (Catelan et al. 2006). Time-series observations in B and V were obtained with the Warsaw 1.3m telescope at the Las Campanas Observatory (LCO), in the course of 7 consecutive nights over the period April 6–13 2003. The camera used is the 8kMOSAIC camera, comprised of eight 2040×4096 chips, with a scale $0.26''/\text{pixel}$ giving an observing area equal to $35' \times 35'$. The cluster was roughly centered on chip 2, and so in this paper we focus our analysis on this chip (which covers a sky area of $8.8' \times 17.8'$). The monitored field on chip 2 covers most of the cluster area, as the tidal radius of M62 is estimated at $r = 8.95$ arcmin (Trager et al. 1995) or $r = 10.01$ arcmin (Beccari et al. 2006). The read out noise of the camera is 6 to $9 e^-$ (depending on the chip) and the gain is $6.3 e^-/\text{ADU}$. A total of 126 images in B and 126 in V were secured with this setup. During the nights of the observations, the seeing was stable enough with an average measured stellar point-spread function (PSF) on the

frames of about $0.98''$ FWHM. Exposures times ranged from 100 s to 220 s for the B frames and 30 s to 90 s for the V frames.

Observations of the standard fields PG+0918, PG+1323, PG+1525, PG+1528, PG+1633, PG+1657 and Ru 152 (Landolt 1992) were obtained on the same nights, to calibrate the data to the standard Johnson-Cousins photometric system. In order to provide better sampled light curves, the Warsaw data were complemented by observations obtained with the Cerro Tololo Inter-American Observatory (CTIO) 1.3m telescope in service mode, using the ANDICAM 1024×1024 CCD, with a scale $0.369''/\text{pixel}$, over the timespan April 24 2003 to June 30 2003. This additional dataset consists of 42 images in each of B and V , and permitted us to extend the time interval spanned by our observations up to about three months, thus resulting very useful to pin down periods and to search for long-term variability. The exposure times in this case were 145 s for the B frames and 40 s for the V frames. The seeing during these observations was on average $\sim 1.3''$, with stable and good photometric conditions. However, no standard fields were observed with the CTIO 1.3m telescope. The LCO images were pre-processed with the Warsaw 1.3m

Table 2
Photometry of the Variable Stars

Name	Filter	JD (d)	Phase	Mag (mag)	e_Mag (mag)
V01	V	2,452,736.54861	0.0000	16.2351	0.0031
V01	V	2,452,736.55367	0.0080	16.2779	0.0042
V01	V	2,452,736.55977	0.0176	16.2787	0.0051
V01	V	2,452,736.57490	0.0414	16.3361	0.0054
V01	V	2,452,736.58749	0.0612	16.3878	0.0059
V01	V	2,452,736.59664	0.0756	16.3996	0.0059

Note. — This table is published in its entirety in the electronic edition of the *Astronomical Journal*. A portion is shown here for guidance regarding its form and content.

pipeline, so that no additional pre-reduction steps were necessary. The preliminary reduction of the CTIO frames, including bias subtraction and flat fielding, were carried out using the standard IRAF⁶ data reduction package.

Since no photometric calibration was obtained during the CTIO run, we used the well calibrated LCO set to link the CTIO instrumental magnitudes to the standard Johnson system. With this purpose in mind, we performed a cross correlation between the LCO and the CTIO catalogues, and then selected the best 50 stars in common that covered a sufficiently wide range in color to prevent any residual uncorrected color trend. These selected stars were then used to calibrate the CTIO data by means of a least-squares fit.

We will provide further detailed information regarding our calibration in Paper II (Contreras et al. 2010, in preparation), when a detailed analysis of our derived cluster CMD will also be provided. In any case, we note that our derived calibration equations are well defined, and have zero point errors of only about 0.006 mag in *B* and 0.011 mag in *V*, with similarly small errors in the derived color coefficients.

3. VARIABLE STARS IDENTIFICATION AND PERIOD DETERMINATION

Since the pioneering effort by Tomaney & Crots (1996), it became clear that the image subtraction technique is one of the best tools for identifying variable stars in crowded fields like globular clusters, due to its powerful capability of comparing images after all non-variable objects have been removed. We have selected the ISIS v2.2 package for this purpose (Alard 2000). The ISIS reduction procedure that we follow consists of several steps: (1) We transform all the frames to a common coordinate grid, where the image taken with the best seeing was chosen as astrometric reference; (2) We select 10% of our frames with the best seeing conditions to construct a composite, reference photometric image; (3) We then subtract each individual frame from the composite image, after convolving the latter so that both images end up having similar PSF's. As the flux of non-variable stars on both images should be essentially identical, such objects will disappear when one image is subtracted from the other, and the remaining signal will (ideally) come exclusively from variable stars; (4) We construct a median image of all the subtracted images (known as “var.fits”) in order to enhance these weak individual (residual) signals, and thus making variable stars candidates more easily identifiable as significant peaks in the median image; (5) Finally, profile-fitting photometry was per-

⁶ IRAF is distributed by the National Optical Astronomy Observatories, which are operated by the Association of Universities for Research in Astronomy, Inc., under cooperative agreement with the National Science Foundation.

Table 3
Fourier Coefficients for RRc Variables in M62

ID	A_{21}	A_{31}	A_{41}	ϕ_{21}	ϕ_{31}	ϕ_{41}
V30	0.124	0.068	0.039	4.514	3.298 ± 0.120	2.196
V40	0.144	0.078	0.057	4.932	3.624 ± 0.083	2.188
V42	0.056	0.023	0.023	4.159	0.825 ± 0.448	0.581
V53	0.163	0.096	0.080	4.761	2.976 ± 0.080	1.709
V65	0.081	0.038	0.058	4.954	4.192 ± 0.407	2.908
V66::	0.740	0.647	0.540	6.262	6.243 ± 0.009	6.259
V69	0.067	0.057	0.032	4.673	3.936 ± 0.154	2.960
V77:	0.133	0.138	0.073	6.268	4.013 ± 0.166	2.574
NV85	0.074	0.069	0.020	4.903	4.001 ± 0.120	1.797
NV86	0.133	0.081	0.037	4.534	3.561 ± 0.106	2.417
NV90:	0.143	0.028	0.071	5.017	3.616 ± 0.455	2.751
NV91	0.100	0.074	0.030	4.875	3.972 ± 0.116	2.817
NV100	0.176	0.077	0.061	4.641	2.794 ± 0.089	1.703
NV101	0.063	0.054	0.049	5.314	3.592 ± 0.194	2.700
NV108	0.112	0.089	0.013	4.542	3.602 ± 0.115	2.150
NV110	0.085	0.087	0.066	5.124	4.118 ± 0.104	2.866
NV111::	0.046	0.086	0.093	4.375	4.317 ± 0.106	0.925
NV115	0.184	0.075	0.052	4.711	2.807 ± 0.079	1.773
NV118	0.115	0.074	0.046	4.633	3.505 ± 0.106	2.446
NV119	0.090	0.056	0.043	4.440	3.793 ± 0.149	2.296
NV121	0.064	0.083	0.036	4.642	3.138 ± 0.133	2.480
NV123	0.101	0.075	0.041	4.512	3.839 ± 0.130	2.705
NV128:	0.187	0.025	0.021	3.889	1.897 ± 0.492	0.922
NV131	0.095	0.079	0.039	5.002	3.764 ± 0.131	2.308
NV132	0.096	0.042	0.030	4.058	4.687 ± 0.258	2.598
NV133:	0.115	0.071	0.050	4.675	4.236 ± 0.162	2.321
NV140	0.035	0.079	0.028	5.767	4.863 ± 0.134	3.072
NV153	0.113	0.051	0.037	4.894	3.688 ± 0.150	2.227
NV175	0.136	0.101	0.049	4.558	3.055 ± 0.083	1.833
NV192	0.090	0.028	0.026	4.788	2.338 ± 0.398	1.210
NV202	0.131	0.046	0.037	4.878	2.782 ± 0.413	0.751
NV204:	0.176	0.084	0.081	4.028	2.769 ± 0.214	5.780
NV221:	0.120	0.110	0.071	5.602	4.185 ± 0.121	3.345
NV224	0.109	0.088	0.036	4.735	3.653 ± 0.131	1.639
NV225:	0.145	0.091	0.113	4.341	4.403 ± 0.197	2.116
NV229:	0.060	0.037	0.005	4.846	4.208 ± 0.450	0.562

formed for each variable star candidate on the subtracted images.

Periods were determined using the phase dispersion minimization (PDM) method Stellingwerf (1978), as implemented in IRAF. PDM is a generalization of the Lafler & Kinman (1965), and essentially attempts to identify the phased light curve that produces the minimum scatter in phase. We were thus able to detect and confirm the existence of at least 245 variable stars in the field of M62, including 209 RR Lyrae, 4 type II Cepheids, 25 LPV's, 1 eclipsing binary, and 6 of uncertain nature. Among the detected RR Lyrae, 133 are fundamental-mode (RRab or RR0) pulsators, whereas 76 are first-overtone (RRc or RR1) stars. We must stress that just 1 out of the 8 Warsaw 1.3m chips were analyzed, and so the total number of (undiscovered) variable stars in the cluster is almost certainly higher. Indeed, although the Beccari et al. (2006) profile suggests that we should find $\approx 98.6\%$ of all cluster stars within $185''$ of the cluster center, we find clear evidence for an excess of variable stars whose properties are consistent with cluster membership further out. More specifically, in chip 2 we find about 4 times more variable stars outside $185''$ than predicted by the cluster's density profile. More details are provided in §5. The remaining chips will be the subject of a future paper, where the possible existence of extra-tidal stars in this cluster will also be examined. Finding charts for the M62 variable stars are presented in Figure 1.

We identified 66 of the 83 known variable stars discovered in previous studies (see the online catalogue by Clement et al. 2001, for a listing). Of the remaining 17 stars, we were un-

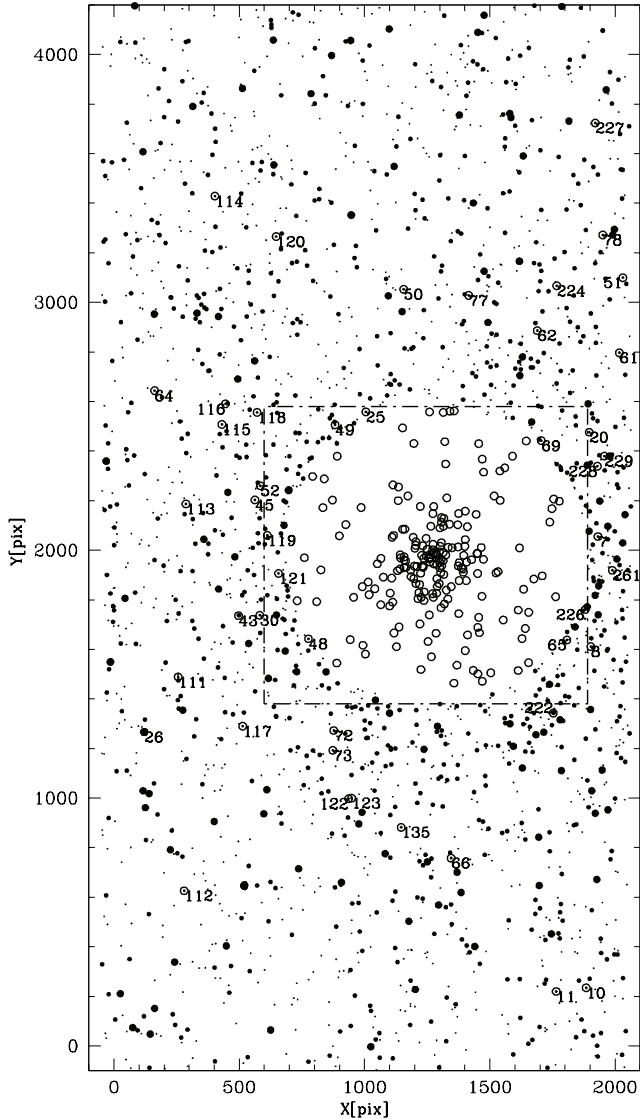


Figure 1. Finding chart for the variable stars in M62, based on the Warsaw 1.3m chip containing the cluster center. A zoom in around the dot-dashed region is shown in the next panel.

able to confirm variability for 2 of them, whereas the other 15 stars fall outside the fields that we have analyzed. On the other hand, Malakhova et al. (1997) find an additional 43 stars that they claim to lie in the instability strip of the cluster, and which are accordingly RR Lyrae candidates. In our study we were able to confirm the variability of 27 among their 43 candidates, with the remaining 16 stars being non-variable in our data.

Taking into account the 209 RR Lyrae stars detected in our study and the 15 additional RR Lyrae stars listed in Clement et al. (2001) which fall outside our studied fields, this gives a total of 224 RR Lyrae stars that are known so far in this cluster. For comparison, the most RR Lyrae-rich (in the sense of total number of RR Lyrae stars present) globular cluster known in our galaxy, M3 (NGC 5272), possesses a total of 230 reported RR Lyrae stars (Clementini et al. 2004), being followed by ω Centauri (NGC 5139), with a total of 178 RR Lyrae (Clement et al. 2001). Clearly, our detections place M62 among the most RR Lyrae-rich globular clusters known, and further analysis of the outer fields not included

in our study is not unlikely to give it the title of the most RR Lyrae-rich of all known globular star clusters (see also Contreras et al. 2005). In terms of the specific frequency of RR Lyrae variables, given by $S_{RR} = N_{RR} \times 10^{0.4(7.5+M_V)}$, and using for the cluster a $M_V = -9.19$ (as given in the Harris 1996 catalog, Feb. 2003 update), one finds $S_{RR} = 47.2$, which is very similar to the value $S_{RR} \approx 46$ originally reported by Contreras et al. (2005), and which again confirms the fact that M62 is an extremely RR Lyrae-rich object, since there are at present only 9 clusters with higher known S_{RR} , again according to the Harris catalog. In this sense, also noteworthy is the large number of LPV stars detected in the M62 field, with a total of 25 variables, 18 of which appear to be likely cluster members (see §5). According to the Clement et al. catalogue, previously the most LPV-rich of all globular clusters was ω Cen, with a total of 15 LPV stars. This suggests that M62 may also be the most LPV-rich known of all globular clusters (again in the sense of total number of LPV stars present).

While ISIS is very efficient in detecting variable stars in crowded fields, it presents the drawback of providing light curves in flux values relative to the composite frame. For this reason, ISIS does not provide light curves in standard magnitudes, and the composite image has to be processed independently for this purpose. To put our light curves in standard magnitude units, we followed the procedure recommended by Mochejska et al. (2001), for those variable stars which could be reliably measured in the reference frame. More specifically, the variable stars detected by ISIS were counter-identified with the B , V master catalogue of the reference frame, as obtained with DAOPHOT/ALLFRAME (Stetson 1987, 1994). Then, following the same procedure as in Mochejska et al., this allowed us to transform the light curves from differential fluxes into magnitude units.

While DAOPHOT/ALLFRAME represents an excellent tool to perform absolute photometry in the crowded regions found in globular clusters, it is still often the case that the variable stars located in the very crowded cluster center, as well as those located near bright and/or saturated objects (or close to the edges of the frames) will lack reliable photometry, even in our best seeing (reference) images. Therefore, among our sample of variable stars, 110 objects have differential flux light curves only, either because we could not measure their magnitudes on the reference frames, or because we consider that they lack reliable DAOPHOT/ALLFRAME photometry due to one or more of the aforementioned reasons.

Photometric properties and basic elements for the 245 variable stars in our study are presented in Table 1. Column 1 indicates the star's ID. Columns 2 and 3 provide the right ascension and declination (J2000 epoch), respectively, whereas column 4 gives our derived periods. Columns 5 and 6 list the derived amplitudes in the B and V bands, respectively. Columns 7 and 8, give the intensity-weighted mean B and V values, while column 9 shows the magnitude-weighted mean color. In column 10 we provide our derived reddening values for individual RRab stars (see §5 for more details), and finally column 11 indicates the star's variability type. We assigned a prefix "NV" to the newly identified objects, including the variable star candidates (NV84-NV110) from Malakhova et al. (1997). For the previously known 66 confirmed variables in our field, we obtain revised periods based on our data alone, since these new periods produce less scattered light curves than the old ones. The exception are

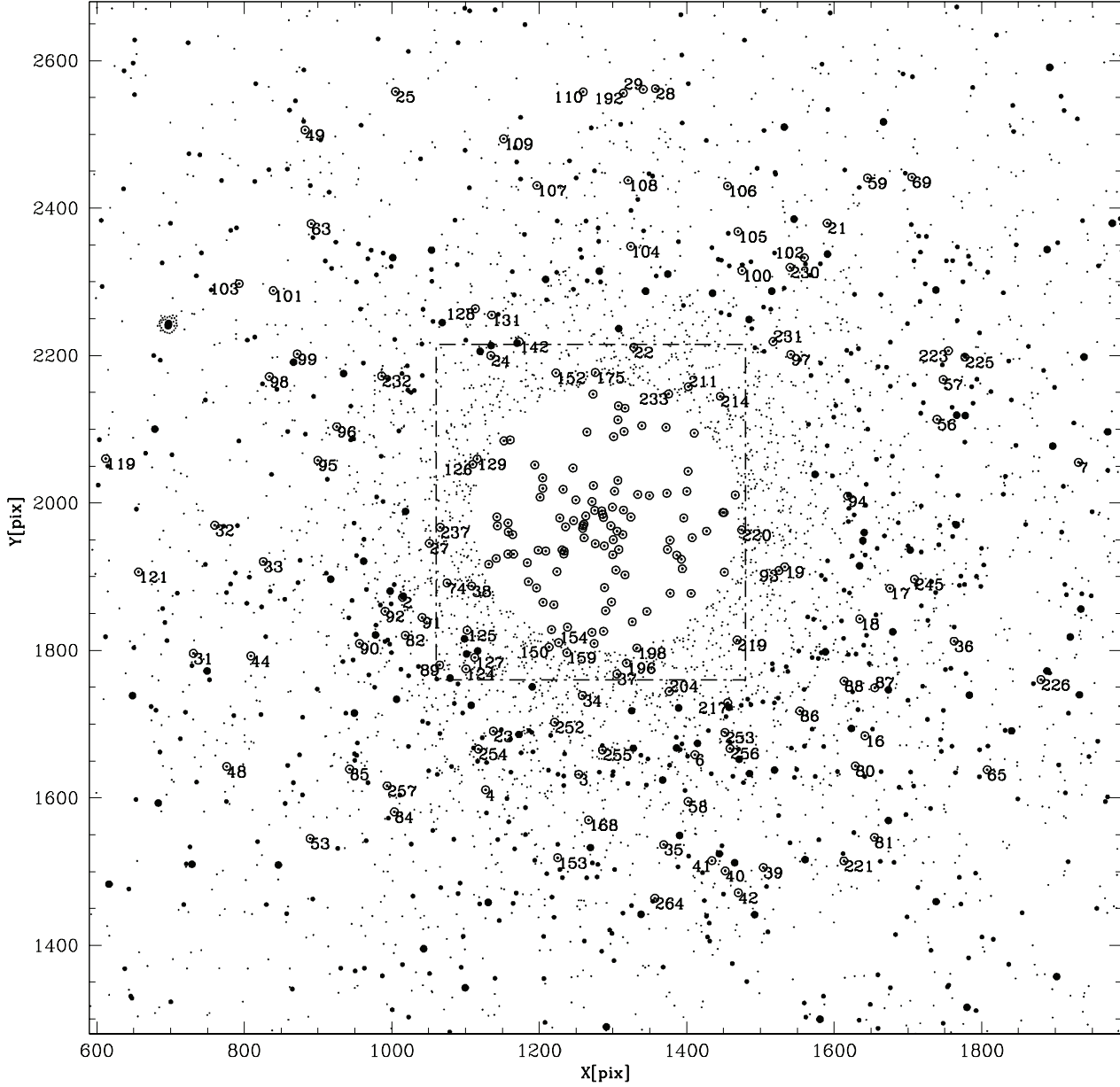


Figure 1, cont. Finding chart for the variable stars in M62. A zoom in around the dot-dashed region is shown in the next panel.

variables V4, V10, V11, V20, V23, V27, V38, V43, V45, V50, V52, V62, V64, V66 and V78, where we adopt periods from the Clement et al. (2001) online catalog, since they provide good matches to our data. Sample light curves for the newly detected variables stars are shown in the Appendix, whereas the complete set of light curves can be found in the electronic version. The light curve data are provided, in machine-readable form, in Table 2.

3.1. Notes on Individual Variable Stars

V1, V3: Periods for these stars are not provided in the online Clement et al. (2001) catalog. The derived periods are based on an analysis of the CTIO images, even though only the LCO photometry is shown in the electronic version of the Appendix.

V77, NV117, NV149, NV155, NV166, NV174, NV176, NV178, NV186, NV197, NV202, NV204, NV207, NV225, NV229: These are short-period RRc stars with seemingly

variable light curves. We have not been able to identify any source of spurious error in our photometry that could affect these stars in particular.

NV92, NV103, NV124, NV126, NV129, NV167, NV182, NV200, NV203, NV211, NV220: The derived periods are based on an analysis of the CTIO images, even though only the LCO light curves, which present significantly less scatter but do not constrain these stars’ periods as tightly, are shown in the Appendix.

NV112, NV120, NV137, NV187, NV194: These stars present several aliases, and could not be detected in the CTIO data. The periods adopted are the ones that appear most consistent with an RRab type.

NV134, NV149: These stars present several aliases, and could not be detected in the CTIO data. The periods adopted are the ones that appear most consistent with an RRc type.

NV159, NV169: These stars show a curious mismatch in the light curves around phase 0.8 for the adopted periods. How-

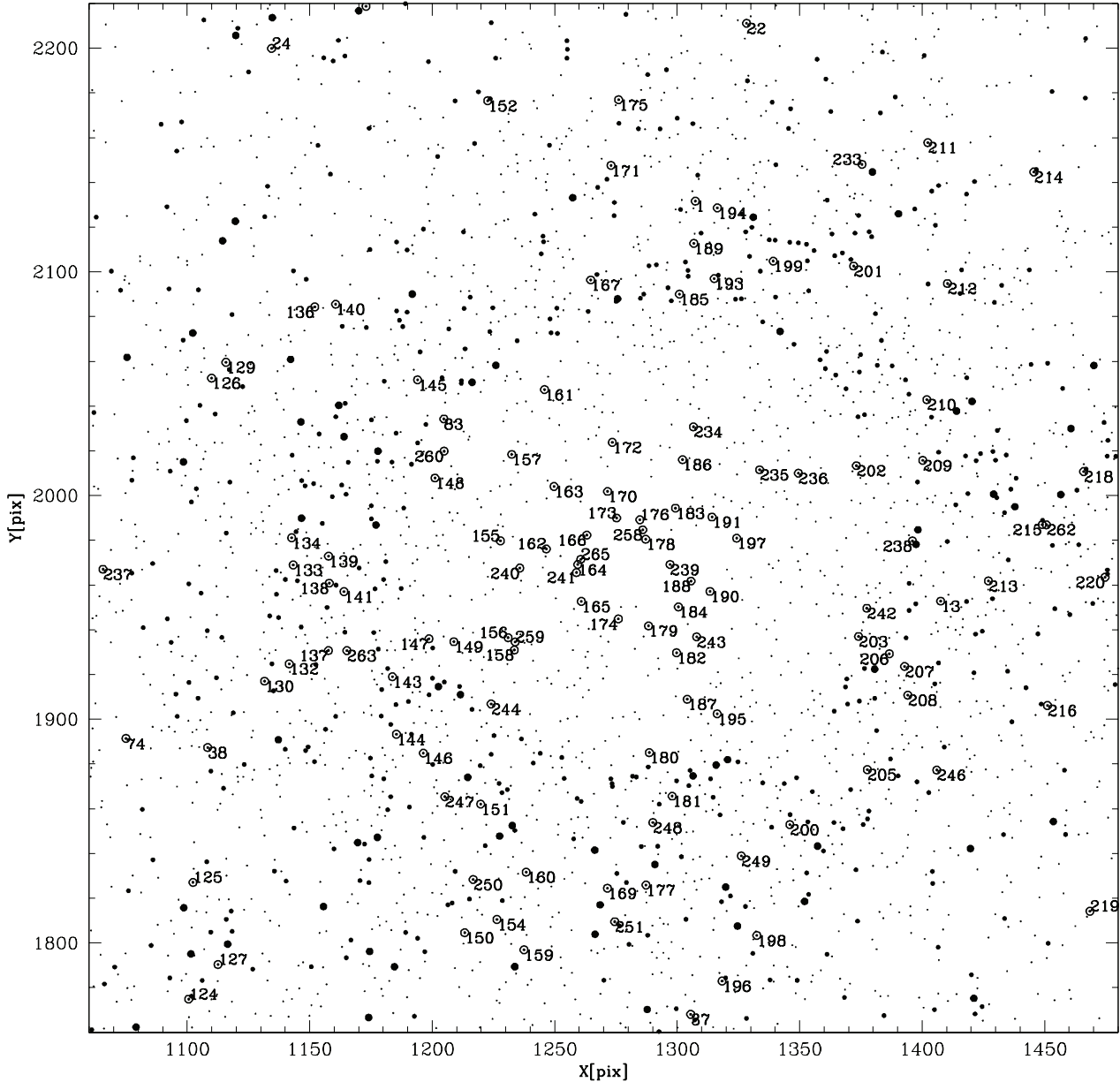


Figure 1, cont. Finding chart for the variable stars in M62 (innermost region).

ever, the latter are confirmed on the basis of the CTIO data.

NV170: This star presents several aliases, and an uncertain classification.

NV215: This star’s light curve presents an unusual behavior close to minimum light. A similar behavior is found in both the LCO and CTIO datasets, though the latter is considerably more noisy and contains fewer datapoints.

4. FOURIER DECOMPOSITION

In the Fourier decomposition method, the light curves of ab-type pulsating stars are frequently fitted with a Fourier series of the form

$$mag = A_0 + \sum_{j=1}^n A_j \sin(jwt + \phi_j), \quad (1)$$

where $w \equiv 2\pi/P$. The light curve shape is then quantified in terms of the lower-order ($j = 2-4$) coefficients $A_{j1} = A_j/A_1$

and $\phi_{j1} = \phi_j - j\phi_1$. In the case of c-type RR Lyrae, a similar procedure is followed, but a cosine decomposition is frequently used instead. In our study, we performed such Fourier decomposition of the RR Lyrae light curves, using $n = 10$, and adopting a sine series for the RRab and a cosine series for the RRc stars. Amplitude ratios A_{j1} and phase differences ϕ_{j1} for the lower-order terms are provided in Tables 3 and 4 for the RRc and RRab stars, respectively. For the RRab stars we also give the Jurcsik-Kovács D_m value (Jurcsik & Kovács 1996, computed on the basis of their eq. 6 and Table 6), which is intended to differentiate RRab stars with “regular” light curves from those with “anomalous” light curves, such as those presenting the Blazhko effect (but see Cacciari, Corwin, & Carney 2005, for a critical discussion of D_m as an indicator of the occurrence of the Blazhko phenomenon). In these tables, a colon symbol (“:”) indicates an uncertain value, whereas a double colon (“::”) indicates a very uncertain value, the latter being provided for complete-

ness only. The error in the ϕ_{31} coefficient was obtained from equation (16d) of Petersen (1986).

4.1. RRc Variables

Simon & Clement (1993) demonstrated, based on hydrodynamical models, that Fourier decomposition of RRc light curves can potentially provide a very useful technique for determining physical parameters of these stars. As a matter of fact, they have provided equations relating the masses, luminosities, temperatures, and even a “helium abundance parameter” of c-type RR Lyrae stars to their periods and ϕ_{31} values. Although these equations have been widely used in literature they must be used with some caution, since a combination of their equations for the RR Lyrae masses and luminosities gives results that are inconsistent with the period-mean density equation of stellar pulsation theory (Catelan 2004b; Deb & Singh 2010). Accordingly, while we still provide luminosities, masses and temperatures derived on the basis of the Simon & Clement relations, we warn the reader that these quantities cannot all be simultaneously valid, and should accordingly be used for comparison with similar work for other GCs only.

Based on the Simon & Clement (1993) relations, we find that an error of 0.2 in ϕ_{31} leads to an error of $\sim 0.03 M_{\odot}$ in mass and ~ 0.03 mag in (bolometric) magnitude, and so we apply this method only to RRc stars with errors in ϕ_{31} of 0.2 or less. We thus computed values of M/M_{\odot} , $\log(L/L_{\odot})$, $\log T_{\text{eff}}$, and “helium abundance parameter” y (which, as is well known, is not necessarily equal to the helium abundance Y ; see, e.g., Corwin et al. 2003); the resulting values are provided in Table 5, where we also provide $[\text{Fe}/\text{H}]_{\text{ZW84}}$ values (in the Zinn & West 1984, scale), based on the calibration recently provided by Morgan, Wahl, & Wieckhorst (2007), and M_V values, based on the calibration by Kovács (1998).

As the reader will readily notice, many of the mass values given in Table 5 are too low, approaching the mass of the degenerate helium core at the He flash ($\simeq 0.5 M_{\odot}$; see Catelan 2009, for a recent review). Such low mass values, which are not uncommon in the literature (e.g., Corwin et al. 2003, and reference therein) likely confirm the existence of a problem with the Simon & Clement (1993) calibration equations.

For the 21 retained RRc stars the unweighted mean values and standard deviations of the mass, log luminosity, effective temperature and helium parameter are $(0.533 \pm 0.04) M/M_{\odot}$, 1.663 ± 0.01 , (7413 ± 34) K, and 0.293 ± 0.003 , respectively. The mean metallicity, in turn, is found to be $[\text{Fe}/\text{H}]_{\text{ZW84}} = -1.23 \pm 0.09$.

According to the Kovács (1998) calibration, the mean absolute magnitude in V of these RRc stars turns out to be $\langle M_V \rangle = 0.714 \pm 0.033$. Since for these stars we also have a $\langle V \rangle = 16.44 \pm 0.06$ mag (standard error of the mean), this gives for the cluster an apparent distance modulus of $(m - M)_V = 15.73 \pm 0.068$ mag.

4.2. RRab Variables

In a series of papers, the Hungarian team has provided a calibration of several physical parameters of “well-behaved” (as indicated by the aforementioned D_m parameter) ab-type RR Lyrae stars as a function of their Fourier decomposition parameters (e.g., Jurcsik & Kovács 1996; Jurcsik 1998; Kovács & Walker 1999, 2001). Unlike the approach adopted by Simon & Clement (1993) for the RRc stars, their method does not rely on hydrodynamical models for the calibration. Following the same approach as described in detail in

Table 4
Fourier Coefficients for RRab Variables in M62

ID	A_{21}	A_{31}	A_{41}	ϕ_{21}	ϕ_{31}	ϕ_{41}	D_m
V4	0.452	0.315	0.256	2.392	4.780	1.046	4.9
V6:	0.455	0.301	0.220	2.351	4.929	1.237	2.7
V7	0.523	0.341	0.200	2.638	5.468	2.141	2.2
V8	0.520	0.356	0.218	2.354	5.130	1.563	3.5
V10	0.511	0.351	0.234	2.363	5.101	1.526	1.2
V11::	0.452	0.228	0.138	2.738	5.493	1.910	6.1
V16	0.500	0.336	0.171	2.624	5.368	2.132	5.9
V17	0.555	0.380	0.251	2.369	5.059	1.556	3.
V18	0.492	0.340	0.221	2.378	5.153	1.645	3.1
V20	0.476	0.394	0.257	2.281	4.878	1.087	3.4
V21	0.476	0.364	0.221	2.218	4.772	1.032	2.4
V23	0.547	0.392	0.238	2.084	4.474	0.628	42.9
V24	0.508	0.344	0.264	2.377	5.204	1.608	6.2
V25	0.473	0.343	0.216	2.225	4.796	1.142	1.7
V26	0.569	0.288	0.186	2.519	5.227	1.701	2.9
V27	0.478	0.353	0.224	2.288	4.891	1.261	2.5
V28::	0.786	0.321	1.381	0.782	5.934	5.959	1617.8
V29	0.535	0.317	0.251	2.422	5.142	1.620	4.6
V31:	0.523	0.381	0.236	2.268	4.947	1.152	4.
V32	0.517	0.330	0.221	2.466	5.297	1.863	1.7
V33	0.549	0.341	0.209	2.523	5.313	2.004	2.5
V34	0.529	0.314	0.188	2.559	5.264	1.868	1.3
V35	0.487	0.339	0.223	2.363	5.076	1.557	0.6
V36	0.459	0.278	0.105	2.646	5.617	2.238	2.9
V39	0.429	0.211	0.080	2.610	5.735	2.845	7.2
V41	0.495	0.306	0.177	2.529	5.391	2.071	1.6
V43	0.529	0.342	0.212	2.433	5.177	1.736	2.2
V44	0.392	0.211	0.092	2.370	4.808	0.977	46.9
V48	0.444	0.271	0.088	2.812	5.914	2.697	127.6
V49	0.517	0.313	0.197	2.338	5.090	1.596	1.
V50::	1.070	1.287	1.461	1.771	3.458	5.002	590.
V52::	1.178	1.808	2.167	1.873	3.279	4.364	3585.7
V56	0.501	0.314	0.194	2.472	5.314	1.902	1.5
V57	0.478	0.304	0.170	2.441	5.197	1.637	2.1
V58::	1.058	0.888	0.674	4.873	3.491	2.047	204.9
V59	0.531	0.334	0.191	2.567	5.404	2.086	2.8
V62	0.516	0.330	0.212	2.423	5.184	1.693	1.5
V63	0.461	0.264	0.102	2.741	5.692	2.740	5.6
V64:	0.450	0.287	0.163	2.266	4.611	1.000	7.1
V72	0.418	0.231	0.121	2.349	5.051	1.265	39.6
V78:	0.491	0.318	0.168	2.682	5.546	2.297	3.9
V80:	0.445	0.229	0.138	2.541	5.285	2.428	18.
V81	0.528	0.360	0.216	2.411	5.153	1.634	1.7
V82	0.489	0.292	0.145	2.536	5.400	2.278	2.7
NV84	0.388	0.170	0.043	2.774	5.980	2.844	109.
NV87	0.288	0.115	0.059	2.774	5.846	3.653	118.9
NV88	0.496	0.301	0.137	2.608	5.508	2.222	1.7
NV93	0.519	0.368	0.230	2.429	5.132	1.648	2.
NV95:	0.466	0.342	0.203	2.138	4.648	0.846	45.6
NV96	0.481	0.359	0.224	2.259	4.924	1.232	2.8
NV97	0.509	0.313	0.203	2.445	5.274	1.820	2.1
NV98	0.501	0.328	0.207	2.486	5.323	1.812	1.8
NV99::	0.426	0.259	0.149	2.753	6.272	3.011	11.7
NV102	0.421	0.229	0.103	2.646	5.465	2.292	1.3
NV103::	0.872	0.726	0.556	4.808	3.251	1.729	298.9
NV105	0.540	0.363	0.259	2.371	5.087	1.546	4.9
NV106	0.424	0.302	0.220	2.336	4.881	1.328	4.2
NV107	0.479	0.307	0.140	2.555	5.462	2.088	3.6
NV109:	0.461	0.293	0.144	2.626	5.606	2.385	8.8
NV112::	0.936	0.839	0.730	1.672	3.466	5.340	2030.9
NV113::	0.359	0.448	0.176	2.170	4.619	1.514	16.7
NV116	0.375	0.165	0.066	2.643	5.776	2.954	7.8
NV120::	0.872	0.741	0.649	1.613	3.284	4.894	1632.9
NV124::	0.815	0.698	0.548	4.734	3.247	1.697	276.1
NV127	0.529	0.321	0.248	2.307	5.049	1.395	3.5
NV135	0.460	0.300	0.107	2.636	5.420	2.623	108.4
NV136	0.544	0.330	0.173	2.695	5.440	2.250	7.7
NV150	0.343	0.146	0.019	2.535	5.053	1.546	43.9
NV160	0.525	0.358	0.225	2.394	5.272	1.772	3.2
NV168	0.261	0.088	0.023	2.864	5.627	5.322	115.6
NV194::	0.924	0.775	0.623	1.644	3.280	4.853	762.4
NV198:	0.561	0.319	0.168	2.317	5.101	1.824	8.9
NV210	0.466	0.335	0.183	2.339	4.859	1.265	7.5
NV214	0.502	0.328	0.167	2.489	5.325	1.987	1.8
NV218:	0.443	0.271	0.144	2.253	4.759	0.771	41.9
NV219	0.461	0.249	0.112	2.816	5.976	2.706	7.8
NV223	0.519	0.337	0.208	2.386	5.101	1.584	1.1
NV226	0.511	0.303	0.161	2.663	5.588	2.349	2.2
NV227	0.486	0.326	0.195	2.304	4.796	1.174	44.8
NV228:	0.329	0.113	0.031	2.680	5.805	3.165	132.3

Table 5
Physical Parameters derived for RRc Variables in M62

ID	M/M_{\odot}	$\log(L/L_{\odot})$	$\log T_{\text{eff}}$	y	[Fe/H]	$\langle M_V \rangle$
V30	0.573	1.681	3.868	0.282	-1.418	0.733
V40	0.525	1.658	3.871	0.292	-1.180	0.686
V53	0.588	1.651	3.873	0.290	-1.207	0.699
V69	0.496	1.658	3.870	0.294	-1.136	0.725
NV85	0.492	1.663	3.869	0.293	-1.173	0.719
NV86	0.524	1.646	3.872	0.295	-1.082	0.746
NV91	0.494	1.660	3.869	0.293	-1.154	0.714
NV100	0.608	1.651	3.874	0.289	-1.226	0.736
NV101	0.534	1.666	3.870	0.289	-1.259	0.689
NV108	0.526	1.655	3.871	0.293	-1.161	0.760
NV110	0.490	1.678	3.867	0.288	-1.297	0.652
NV115	0.609	1.654	3.873	0.288	-1.253	0.736
NV118	0.539	1.661	3.870	0.290	-1.224	0.723
NV119	0.519	1.674	3.868	0.288	-1.305	0.719
NV121	0.573	1.654	3.872	0.290	-1.209	0.756
NV123	0.500	1.650	3.871	0.296	-1.075	0.730
NV131	0.517	1.667	3.869	0.290	-1.247	0.703
NV140	0.435	1.694	3.862	0.287	-1.347	0.613
NV153	0.527	1.671	3.869	0.288	-1.293	0.708
NV175	0.586	1.660	3.872	0.288	-1.274	0.734
NV224	0.538	1.683	3.867	0.284	-1.397	0.713
mean	0.533±0.043	1.663±0.012	3.870±0.002	0.290±0.003	-1.234±0.009	0.714±0.033

Table 6
Physical Parameters Derived for RRab Variables in M62

ID	[Fe/H] ₉₅	$\langle M_V \rangle$	$\langle B-V \rangle$	$\log T_{\text{eff}}^{(B-V)}$	$\langle V-I \rangle$	$\log T_{\text{eff}}^{(V-I)}$	$\langle V-K \rangle$	$\log T_{\text{eff}}^{(V-K)}$
V4	-1.527	0.782	0.328	3.814	0.479	3.814	1.110	3.810
V7	-0.725	0.840	0.343	3.815	0.498	3.808	1.057	3.813
V8	-1.011	0.843	0.337	3.815	0.491	3.810	1.058	3.814
V10	-1.049	0.808	0.322	3.819	0.472	3.815	1.044	3.816
V17	-1.089	0.830	0.334	3.815	0.487	3.811	1.064	3.814
V18	-0.934	0.848	0.330	3.818	0.481	3.813	1.041	3.816
V20	-1.023	0.867	0.316	3.822	0.464	3.817	0.991	3.822
V21	-1.047	0.868	0.301	3.828	0.444	3.823	0.974	3.824
V25	-0.993	0.875	0.296	3.830	0.439	3.824	0.969	3.824
V26	-0.012	1.047	0.286	3.842	0.424	3.827	0.824	3.837
V27	-0.882	0.868	0.293	3.831	0.435	3.825	0.952	3.826
V29	-1.170	0.768	0.324	3.817	0.475	3.814	1.082	3.812
V32	-0.869	0.843	0.338	3.815	0.493	3.809	1.059	3.814
V33	-0.980	0.813	0.345	3.812	0.501	3.807	1.097	3.810
V34	-1.104	0.772	0.334	3.814	0.487	3.811	1.101	3.810
V35	-1.065	0.847	0.337	3.815	0.490	3.810	1.069	3.813
V36	-1.004	0.774	0.369	3.803	0.532	3.799	1.164	3.802
V41	-0.802	0.862	0.349	3.812	0.506	3.806	1.078	3.811
V43	-1.114	0.828	0.350	3.809	0.508	3.806	1.110	3.809
V49	-1.122	0.825	0.335	3.815	0.488	3.811	1.083	3.812
V56	-0.919	0.837	0.344	3.813	0.500	3.808	1.081	3.811
V57	-1.048	0.831	0.342	3.813	0.497	3.809	1.084	3.811
V59	-0.892	0.828	0.351	3.810	0.509	3.805	1.096	3.809
V62	-1.021	0.834	0.340	3.814	0.494	3.809	1.076	3.812
V81	-0.970	0.843	0.335	3.816	0.488	3.811	1.052	3.815
V82	-0.821	0.875	0.359	3.809	0.518	3.803	1.107	3.808
NV88	-0.762	0.854	0.357	3.809	0.516	3.803	1.093	3.809
NV93	-1.113	0.824	0.344	3.812	0.500	3.808	1.091	3.811
NV96	-0.930	0.874	0.309	3.826	0.454	3.820	0.979	3.823
NV97	-0.915	0.849	0.343	3.813	0.498	3.808	1.072	3.812
NV98	-0.909	0.836	0.345	3.813	0.501	3.807	1.073	3.812
NV102	-1.089	0.799	0.368	3.803	0.531	3.800	1.181	3.801
NV105	-1.002	0.837	0.327	3.818	0.478	3.813	1.040	3.816
NV106	-1.189	0.811	0.305	3.824	0.451	3.821	1.038	3.817
NV107	-0.781	0.868	0.360	3.809	0.519	3.803	1.090	3.810
NV127	-1.120	0.783	0.310	3.823	0.457	3.819	1.037	3.817
NV160	-0.879	0.810	0.325	3.820	0.476	3.814	1.033	3.816
NV214	-1.043	0.817	0.356	3.808	0.514	3.804	1.124	3.807
NV223	-1.048	0.836	0.333	3.816	0.485	3.812	1.063	3.814
NV226	-0.921	0.782	0.359	3.807	0.519	3.802	1.138	3.805
mean ^a	-0.997±0.144	0.830±0.030	0.336±0.019	3.815±0.006	0.489±0.024	3.811±0.006	1.068±0.049	3.813±0.005

^a Excluding V26.

Corwin et al. (2003), we obtain the metallicities, mean colors, and associated temperatures that are listed in Table 6, for 40 RRab stars with $D_m \leq 5$ (see also Clement & Shelton 1997). Note that V26 is most likely a field star (see §5), and therefore was not taken into account when computing the average values for the cluster, as indicated in this table.

Note that the $[\text{Fe}/\text{H}]$ values derived in this way are actually in the scale of Jurcsik (1995). The latter is related to the more traditional Zinn & West (1984) scale by $[\text{Fe}/\text{H}]_{\text{J95}} = 1.431 [\text{Fe}/\text{H}]_{\text{ZW84}} + 0.880$. Therefore, the mean metallicity $[\text{Fe}/\text{H}]_{\text{J95}} = -0.997$ that was derived for the cluster in Table 6 translates into a metallicity value $[\text{Fe}/\text{H}]_{\text{ZW84}} = -1.31$ in the Zinn & West scale. This agrees very well with the value adopted for the cluster by Harris (1996), namely $[\text{Fe}/\text{H}]_{\text{ZW84}} = -1.29$, in his catalog of globular cluster parameters (2003 update), as well as with the value derived from the RRc by using the Morgan et al. (2007) calibration, namely $[\text{Fe}/\text{H}]_{\text{ZW84}} = -1.23$ (§4.1).

Likewise, we obtain a mean absolute magnitude of $\langle M_V \rangle = 0.83 \pm 0.03$ mag for the RRab stars in the cluster. The faint HB is a reflection of the adoption of the Baade-Wesselink luminosity zero point in the calibration of this method (see Jurcsik & Kovács 1999, for a discussion). For the same set of 39 RRab used to derive this value, we also find $\langle V_{RR} \rangle = 16.260 \pm 0.03$ mag (standard error of the mean), which is also in very good agreement with the value of 16.25 mag adopted in the 2003 edition of the Harris (1996) catalog. This implies an apparent distance modulus of $(m-M)_V = 15.43 \pm 0.04$ mag for M62, which is significantly shorter (by 0.21 mag) than the value provided in the Harris catalog, and by an even wider margin (i.e., 0.3 mag) than the value obtained in §4.1 on the basis of the Kovács (1998) M_V calibration for the c-type RR Lyrae. We ascribe these differences to the faint zero point adopted in the original M_V calibrations. If we adopt instead the more recent calibration of the RR Lyrae absolute magnitude-metallicity relation provided by Catelan & Cortés (2008), and the metallicity value for M62 derived above ($[\text{Fe}/\text{H}]_{\text{ZW84}} = -1.31$), we find $M_V(\text{RR}) = 0.68 \pm 0.14$, and an apparent distance modulus of $(m-M)_V = 15.58 \pm 0.14$, which is much more consistent with the value reported in the Harris catalog (being shorter by only 0.06 mag). Using a reddening value of $E(B-V) = 0.47$ (from Harris 1996) and a standard extinction law with $A_V/E(B-V) = 3.1$, this implies a distance modulus $(m-M)_0 = 14.12 \pm 0.14$, which corresponds to a distance of 6.7 ± 1 kpc.

Note that a distance modulus for the cluster may also be obtained on the basis of our detected type II Cepheids, namely V2 and V73, using equation (3) in Pritzl et al. (2003). In this way, we obtain for distance moduli of $(m-M)_V = 15.04$ and $(m-M)_V = 15.57$ mag, respectively – giving an average distance modulus of $(m-M)_V \approx 15.31 \pm 0.26$ mag. Given the large error bar, this value is not inconsistent with the one derived on the basis of the RR Lyrae stars.

As noted by Contreras et al. (2005), M62 may harbor long-period RRc's (see their Fig. 2), which are exceedingly rare among Galactic globular clusters (see Catelan 2004b, for a review). In order to check the pulsation status of the two candidate long-period RRc stars that we have found in the cluster, namely NV104 and NV171, we have used several diagnostics from Simon & Teays (1982) and Clement & Shelton (1997), who have shown that the RRab and RRc stars occupy distinctly different positions in the A_{21} , ϕ_{21} plane in particular, as well as the Sk (skewness) parameter defined by

Stellingwerf & Donohoe (1987). Figure 2 shows that, for the RR Lyrae with clean light curves in our sample, most of the ab-type RR Lyrae do indeed have values of $A_{21} > 0.3$, and vice-versa for the RRc stars. Similarly, most of the RRc stars have $\text{Sk} < 2$, whereas most of the ab-type RR Lyrae have $\text{Sk} > 2$. As can be seen, in all plots but the one showing ϕ_{31} as a function of $\log P$ one finds that the positions of these two stars are closer to the locus occupied by RRc than RRab stars. The atypical position of NV104 and NV171 in the $\phi_{31} - \log P$ plane is particularly intriguing, in view of the fact that, if these stars are indeed c-type RR Lyrae, their periods would clearly be longer than the vast majority of even the ab-type RR Lyrae in the cluster.

5. CMD AND REDDENING

On the basis of our ALLFRAME reductions, we were able to obtain a deep CMD for M62, which we show in Figure 3. The CMD properties will be discussed in detail in a forthcoming paper (Contreras et al. 2010, in preparation), and we show it here with the main purpose of verifying whether the positions of the variable stars that were detected in our field are consistent with cluster membership – which is clearly confirmed for the vast majority of the stars. One obvious exception is provided by the RRab star V26, which is clearly a foreground field RR Lyrae. That V26 is a field star is also suggested by the near-solar metallicity derived for it on the basis of its Fourier decomposition parameters (see Table 6). The membership status of NV224 and NV227, on the other hand, is less clear, for while their CMD positions suggest that they may be RR Lyrae stars in the cluster background, their Fourier-based metallicities do not clearly point to them as being anomalous. In like vein, their metallicity values, as derived using the Jurcsik (1995) and Morgan et al. (2007) techniques, suggest $[\text{Fe}/\text{H}]$ values of -1.40 (for NV224) and -1.35 (for NV227), neither of which is clearly inconsistent with the cluster's metallicity. The derived $[\text{Fe}/\text{H}]$ value for NV227 should be taken with due caution though, in view of the star's fairly large D_m value (see Table 4).

Unfortunately, as can be seen from Figure 3 (left panel), the cluster CMD is severely affected by differential reddening, which is not unexpected in view of M62's large foreground reddening and low Galactic latitude. On the other hand, the presence of a large number of RR Lyrae variable stars across the face of the cluster can provide us with a handle of this problem, since RR Lyrae stars can themselves provide dependable reddening estimates, particularly on the basis of the colors of the ab-type RR Lyrae at minimum light (e.g., Blanco 1992).

We have applied the Blanco (1992) technique to 71 stars in our RRab sample, and thus obtained a two-dimensional reddening map across the face of the cluster. In this case, we adopted the same $[\text{Fe}/\text{H}]$ value for all the RRab stars, namely $[\text{Fe}/\text{H}] = -1.31$, as derived from Fourier decomposition (§4.2), and which is very similar to the value listed in the Harris (1996) catalog, namely $[\text{Fe}/\text{H}] = -1.29$. We then experimented with several different techniques for interpolating on this map to obtain reddening values for individual cluster stars, finally opting for a LOESS smoother (Cleveland 1979; Cleveland & Devlin 1988). That this provided very good results can readily be appreciated by comparing the differential reddening-corrected CMD (Fig. 3, right panel) with the original one. A zoomed-in plot around the HB region is shown in Figure 4.

We also note the anomalous positions of stars NV225 (an

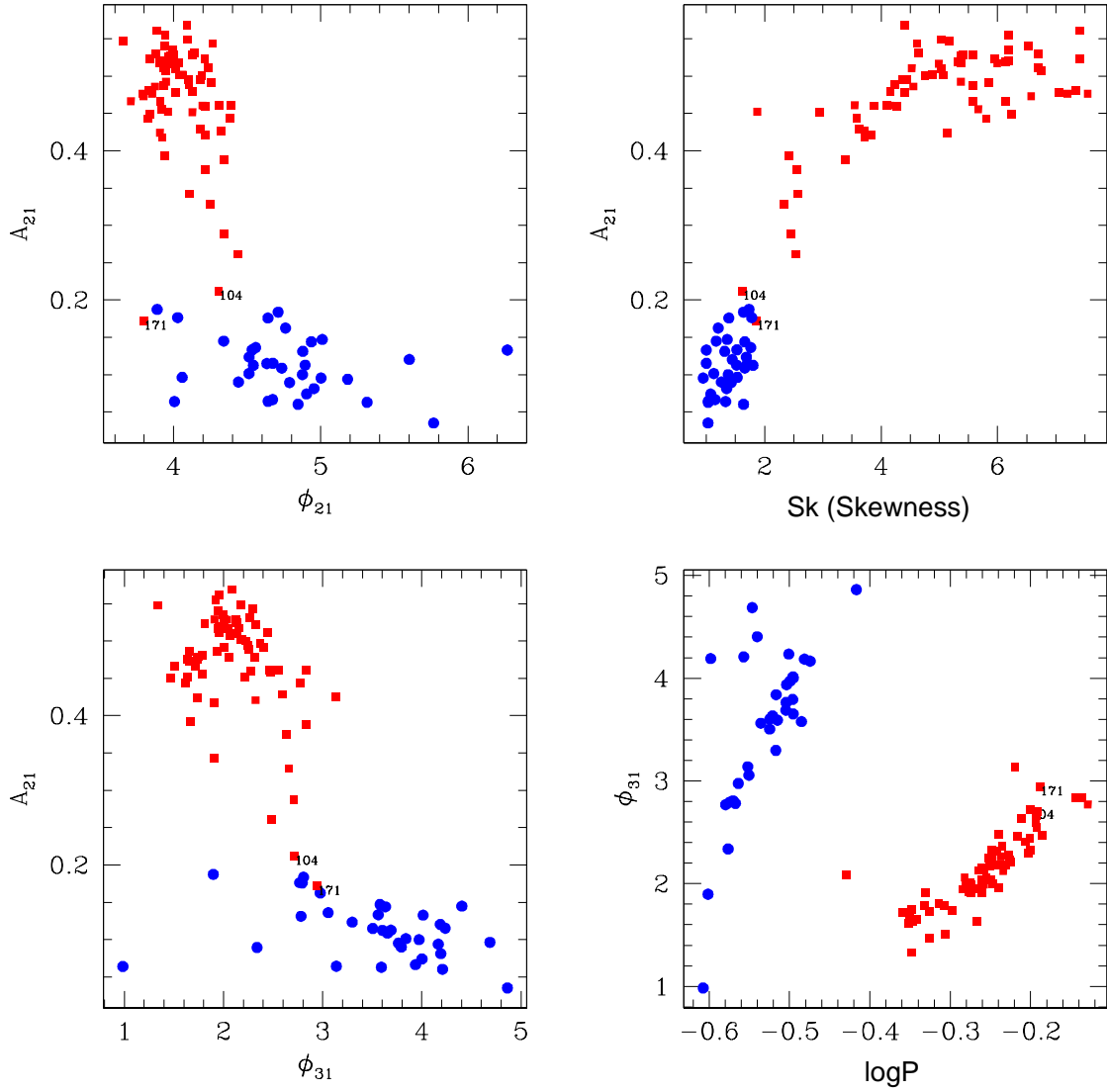


Figure 2. Pulsation mode diagnostics for RR Lyrae stars. In all panels, circles indicate c-type RR Lyrae stars, whereas squares indicate ab-type RR Lyrae. Some of the variables discussed in the text are indicated by their V (or NV) number.

RRc) and V23 (an RRab) in the CMD. Not only are these stars brighter and redder than other RR Lyrae stars in the cluster, but also – and importantly – they also present peculiarly large A_B/A_V amplitude ratios. This strongly suggests that they are blended with redder companions.

In order to verify whether those variable stars for which we were not able to obtain average magnitudes and colors over the full pulsation cycle belong to M62, we have included a third CMD in Figure 5. In this case, the variable stars were simply identified in the photometry catalog and plotted in the CMD using mean magnitudes and colors computed as simple averages of the available photometric data. While this necessarily leads to increased scatter in the derived CMD positions (as is particularly obvious around the RR Lyrae region of the CMD), it also allows us to investigate the likelihood that these stars may be cluster members. To further aid us in this direction, we overplot in Figure 5 two model isochrones from the

Pietrinferni et al. (2006) set, computed for a chemical composition consistent with that of the cluster (in green, reddened and vertically shifted in order to match the HB of the cluster) and for a chemical composition consistent with a bulge field at the position of the cluster (in red, plotted using the same distance modulus as obtained for the cluster). From their CMD positions, it appears that most of the LPV stars discovered in this paper (i.e., 18 out of 25) are likely cluster members, with only a few LPV candidates likely belonging to the bulge. Note also that NV231, which we originally classified as an LPV candidate, may actually be more properly classified as a background type II Cepheid, judging from its position in the CMD.

Finally, we note that all those RR Lyrae stars for which we derived metallicities using Fourier decomposition, and which are located inside the cluster’s tidal radius, present chemical abundances that are compatible with M62 membership, ex-

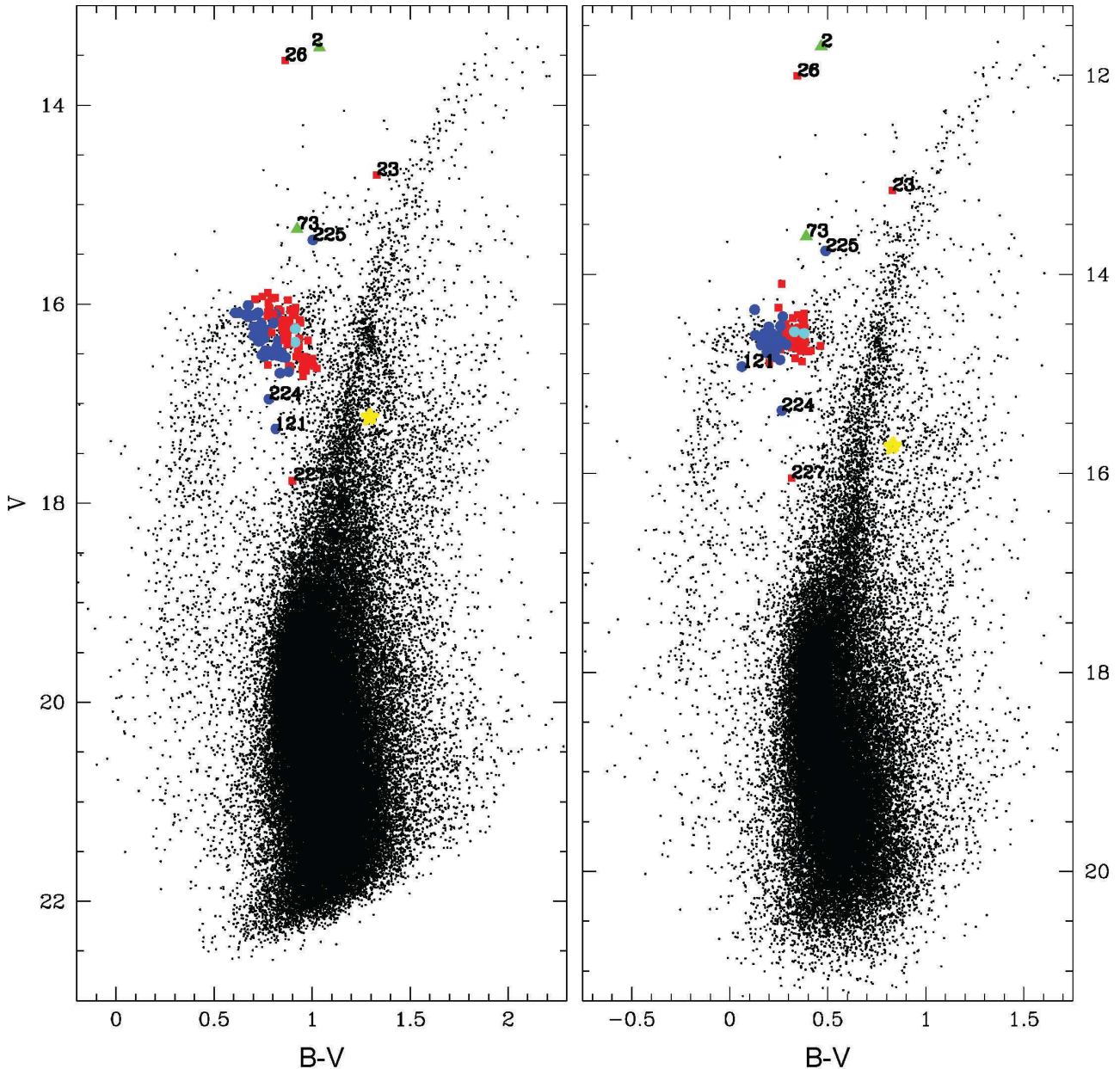


Figure 3. Our derived CMD for the cluster, with the mean values for the detected variable stars overplotted. Circles indicate c-type RR Lyrae, squares ab-type RR Lyrae, and triangles type II Cepheids. The diagram on the right is the same as the one on the left, but with differential reddening accounted for as described in the text.

cept for the already cited case of V26 – thus suggesting that most of the variable star candidates in the cluster outskirts are indeed cluster members.

6. ON THE OOSTERHOFF TYPE OF M62

The Oosterhoff phenomenon is of great astrophysical importance, given the information that it carries on the early formation history of the Milky Way and its neighboring galaxies (e.g., Kuehn et al. 2008; Catelan 2009; Moretti et al. 2009, and references therein), and (increasingly) in the Andromeda system (e.g., Contreras et al. 2008; Clementini et al. 2009; Fiorentino et al. 2010; Sarajedini et al. 2009, and references therein). As recently summarized by Catelan (2009), there is a general tendency for bona-fide Galactic globular clusters to present the so-called Oosterhoff dichotomy, i.e., a sharp division between Oosterhoff type I (OoI) systems, with $\langle P_{ab} \rangle \approx 0.55$ d, and Oosterhoff type II (OoII) systems, with

$\langle P_{ab} \rangle \approx 0.65$ d, with exceedingly few Galactic globulars occupying the range between $0.58 \lesssim \langle P_{ab}(d) \rangle \lesssim 0.62$. On the contrary, nearby extragalactic globular clusters and dwarf galaxies occupy *preferentially* the latter average period interval, thus clearly revealing a difference in (early) formation history between bona-fide Galactic and nearby extragalactic systems.

As discussed by Contreras et al. (2005), there is at present some debate as to whether the Oosterhoff type of a globular cluster is determined chiefly by the morphology of the HB (Clement & Shelton 1999), or whether metallicity plays an important role as well – as would be supported by theoretical calculations that indicate different evolutionary paths for HB stars of different metallicities but similar zero-age HB (ZAHB) temperatures, and thus a different efficiency of production of stars evolved away from the ZAHB as a function of metallicity (see §5.7 in Pritzl et al. 2002, and references

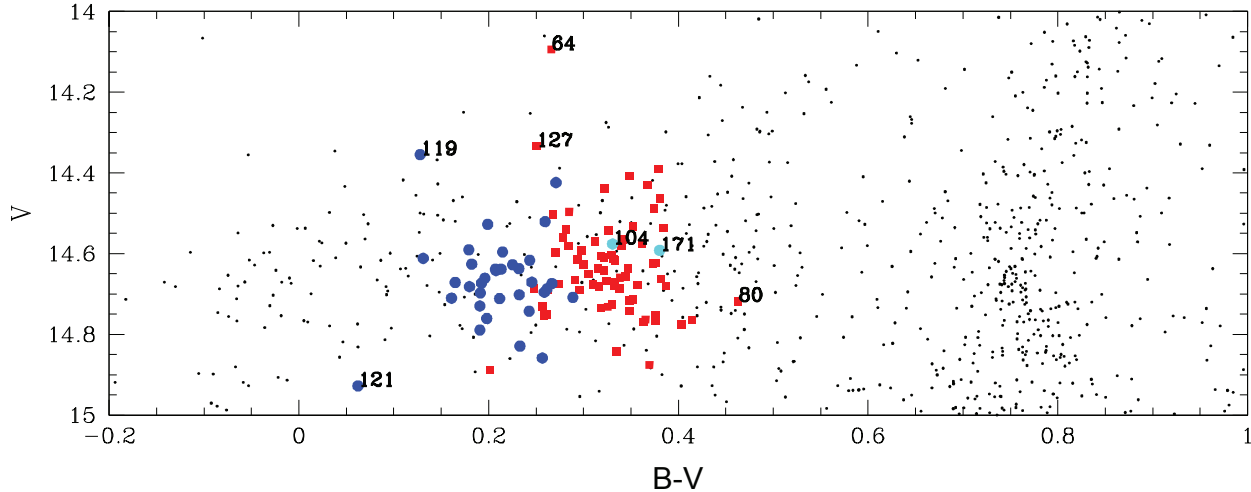


Figure 4. As in Figure 3 (right panel), but zooming in around the HB.

therein). As noted by Contreras et al., M62 provides a near-ideal test of the relative importance of HB morphology and metallicity in defining the Oosterhoff type of a globular cluster, given that the cluster possesses a predominantly blue HB, as in the case of most OoII clusters, but is also a fairly metallic object, as in the case of most OoI clusters.

Here we confirm the preliminary results by Contreras et al. (2005), finding that the mean periods of the ab-type RR Lyrae in M62 support an OoI classification for the cluster, thus clearly showing that, at least in the case of M62, metallicity is the dominant factor that defines the Oosterhoff type. Indeed, let us assume, as a first approximation, that all of our detected variables are cluster members. In this case, and taking our homogeneous sample of 133 RRab's and 76 RRC's into account, we derive for the cluster average pulsation periods of $\langle P_{ab} \rangle = 0.547$ d and $\langle P_c \rangle = 0.302$ d, thus confirming the preliminary values reported by Contreras et al., which are quite typical for OoI systems. If the 5 RRab and 3 RRC with uncertain classification – namely, NV112, NV120, NV137, NV187, NV194 and NV134, NV149 – are removed, we obtain $\langle P_{ab} \rangle = 0.548$ d and $\langle P_c \rangle = 0.301$ d. As we have seen, the membership status for the RRab stars V26 and NV227 and the RRC variable NV224 is also questionable; if we further remove these stars from the final tally, we obtain $\langle P_{ab} \rangle = 0.550$ d (126 RRab stars) and $\langle P_c \rangle = 0.302$ d (73 RRC stars).

As discussed by Catelan et al. (2010, in preparation), $\langle P_{ab} \rangle$ and $P_{ab,min}$ are the two quantities that most strongly define the Oosterhoff type. For M62, the shortest-period RRab is NV188, and thus $P_{ab,min} = 0.436$ d – which again clearly indicates an OoI classification.

As a matter of fact, as shown in Figure 6, the detailed period distribution is quite similar for both the prototypical OoI globular cluster M3 and M62, with the main differences being a somewhat shorter mean period for the RRC stars in M62 and a slightly broader distribution of ab-type periods. The period-amplitude diagram may also provide further insight into these differences, in addition to useful information regarding the Oosterhoff classification of stellar systems (e.g., Cacciari et al. 2005, and references therein). How does this diagram look in the case of M62, once those RRab stars identified as peculiar (i.e., with $D_m > 5.0$) have been removed?

The answer is provided in Figure 7, where both the $A_V - \log P$ (upper panel) and $A_B - \log P$ (lower panel) planes are

shown. In these figures, we also provide reference lines for OoI and OoII globular clusters, as derived by Cacciari et al. (2005) and summarized in eqs. (10)–(15) in Zorotovic et al. (2010). Clearly, there is a tendency for most of the ab-type RR Lyrae to fall around the OoI line in this diagram, which again is fully consistent with an OoI classification for the cluster. The RRC's, on the other hand, appear to have shorter periods, at a given amplitude, than indicated by the reference OoI line, which in turn is based on the M3 RR Lyrae (Cacciari et al. 2005), which is consistent with the pattern observed in Figure 6. A possible interpretation for these differences has been provided by Clement & Shelton (1999), who pointed out that, in the period-amplitude diagram, well-behaved RRab stars of different metallicities seemed to follow a fairly universal mean locus, defined solely by their Oosterhoff types, whereas the RRC's, on the contrary, presented systematic deviations towards shorter periods (at a given amplitude) with increasing metallicity. Given that M62 is more metal-rich than M3, this provides a reasonable explanation for our results.

There is, however, one aspect of the M62 variable star population that may not seem immediately compatible with an OoI classification, namely, the number fraction of c-type variables f_c . It has long been thought that the latter quantity is a strong discriminator of Oosterhoff type, with $f_c \simeq 0.17$ for the OoI systems, and $f_c \simeq 0.44$ for OoII systems (see, e.g., Table 3.2 in Smith 1995). In the case of M62, we find $f_c = 0.363$, which is intermediate between these two reference values, but closer to the one for OoII systems. However, as discussed more recently by Catelan et al. (2010, in preparation), f_c is actually *not* a particularly reliable indicator of Oosterhoff type, with known OoI systems covering a wide range in f_c values, from $f_c \approx 0$ up to 0.65 (with most of the objects falling in the range $0.2 \lesssim f_c \lesssim 0.4$), and likewise known OoII systems covering the range from $f_c \approx 0.1$ up to 0.6 (with most of the objects falling in the range $0.3 \lesssim f_c \lesssim 0.55$). We thus conclude that the f_c value for M62 is not inconsistent with an OoI type classification for the cluster; the fact that it is slightly larger than for most OoI systems is likely due to the fact that M62 also has one of the bluest HB types among OoI globulars.

As discussed by (e.g.) Corwin et al. (2003), the average physical parameters of the c- and ab-type RR Lyrae, as derived on the basis of Fourier decomposition of their light curves, can also provide a useful consistency check of the

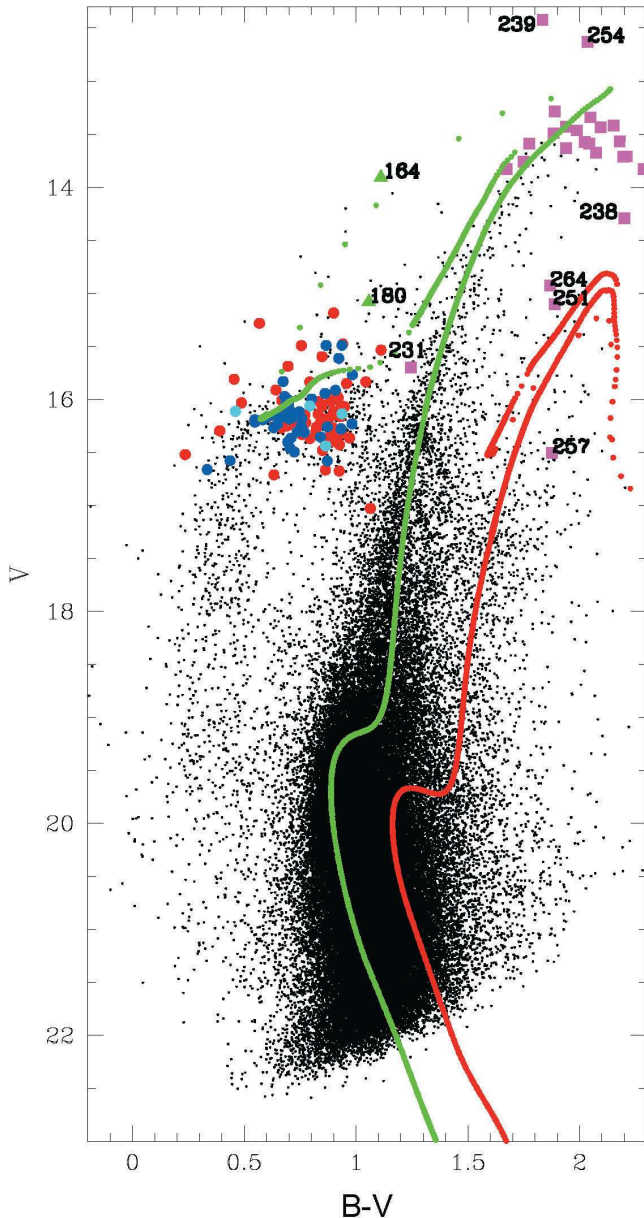


Figure 5. As in Figure 3, but including the variable stars for which the average magnitudes and colors can only be roughly estimated, due to insufficient phase coverage. Filled squares indicate candidate LPV stars. Isochrones for characteristic cluster and bulge chemical compositions are shown as green and red lines, respectively.

derived Oosterhoff type. In Tables 7 and 8 we accordingly compare some of the physical parameters that we derived on the basis of the Fourier decomposition method (§4) with those similarly derived for other clusters in the literature, for the RRC and RRab stars, respectively. As can be seen from these tables, the Fourier-based physical parameters that we derived for M62 are again entirely consistent with an OoI classification for the cluster.

7. THE A -PARAMETER AND THE HE ABUNDANCE IN M62

Recently, several authors have suggested that He abundance enhancements may be quite commonplace among globular clusters (e.g., D’Antona & Caloi 2008). In this scenario, globular clusters with predominantly blue HB morphologies are suggested to be helium rich, and thus it is worthwhile to check the RR Lyrae stars in M62 in search for evidence of He en-

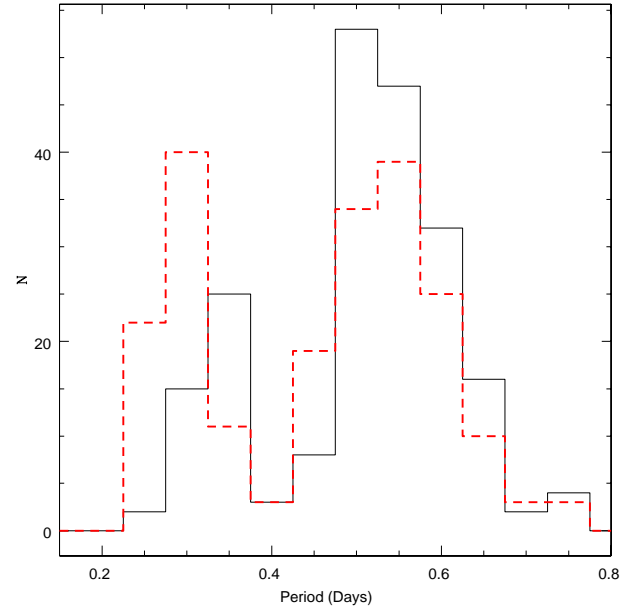


Figure 6. Period histogram for the RR Lyrae stars in M62 (dashed line) and for the RR Lyrae stars in the prototypical OoI globular cluster M3 (solid line).

hancement that might help explain its blue HB.

As is well known, the “ A -method” of Caputo & Castellani (1975) can provide strong constraints on the presence (or otherwise) of He enrichment among RR Lyrae stars. From the period-mean density relation of stellar pulsation theory (van Albada & Baker 1971), one finds

$$\log P = 11.497 + 0.84A - 3.481 \log T_{\text{eff}}, \quad (2)$$

where

$$A \equiv \log(L/L_{\odot}) - 0.81 \log(M/M_{\odot}), \quad (3)$$

with the period in days and the temperature in K. Therefore,

$$A = 13.353 - 1.19 \log P - 4.058 \log T_{\text{eff}}. \quad (4)$$

Similarly, on the basis of the more recent models by Caputo, Santolamazza, & Marconi (1998), Cacciari et al. (2005) obtain

$$A = 13.687 - 1.19 \log P - 4.144 \log T_{\text{eff}}. \quad (5)$$

Thus defined, the A -parameter can therefore be easily computed on the basis solely of period measurements and estimates of the stellar temperatures. As already mentioned, this parameter is strongly sensitive to the He abundance; in particular, according to the ZAHB models of Sweigart & Catelan (1998) for $Z = 0.002$, A depends on Y according to $(dA/dY)_{T_{\text{eff}}, Z} \simeq 1.56$, in the range of Y between 0.23 and 0.28. For comparison, the dependence on Z at fixed Y is much milder, the same models indicating, in the range between $Z = 0.0005$ and $Z = 0.002$, a slope $(dA/d \log Z)_{T_{\text{eff}}, Y} \simeq -0.05$.

Here we provide a comparison with the globular cluster M3, which has been extensively studied previously, and which has a metallicity fairly similar to M62’s. In particular, A -parameter values can be derived for the ab-type RR

Table 7
Mean Parameters for RRc Stars in Globular Clusters (from Fourier Decomposition)

ID	Oo Type	[Fe/H] _{H03} ^a	No. of Stars	M/M_{\odot}	$\log(L/L_{\odot})$	$T_{\text{eff}}(\text{K})$	y
NGC 6362 ^b	I	-0.95	14	0.53	1.66	7429	0.29
NGC 6171 (M107) ^c	I	-1.04	6	0.53	1.65	7447	0.29
NGC 5904 (M5) ^d	I	-1.27	14	0.54	1.69	7353	0.28
NGC 6266 (M62)	I	-1.29	21	0.53	1.66	7413	0.29
NGC 6229 ^e	I	-1.43	9	0.56	1.69	7332	0.28
NGC 6934 ^f	I	-1.54	4	0.63	1.72	7290	0.27
NGC 5272 (M3) ^g	I	-1.57	5	0.59	1.71	7315	0.27
NGC 7089 (M2) ^h	II	-1.62	2	0.54	1.74	7215	0.27
NGC 5286 ⁱ	II	-1.67	12	0.60	1.72	7276	0.27
NGC 6809 (M55) ^j	II	-1.81	5	0.53	1.75	7193	0.27
NGC 4147 ^k	I	-1.83	9	0.55	1.69	7335	0.28
NGC 2298 ^l	II	-1.85	2	0.59	1.75	7200	0.26
NGC 4590 (M68) ^m	II	-2.06	16	0.70	1.79	7145	0.25
NGC 7078 (M15) ⁿ	II	-2.26	8	0.76	1.81	7112	0.24
NGC 6341 (M92) ^o	II	-2.28	3	0.64	1.77	7186	0.26

^a From the Harris (1996) catalog (Feb. 2003 issue).

^b From Olech et al. (2001).

^c From Kaluzny et al. (2000).

^d From Kaluzny et al. (2000).

^e From Borissova et al. (2001).

^f From Kaluzny et al. (2001).

^g From Kaluzny et al. (1998).

^h From Lázaro et al. (2006).

ⁱ From Zorotovic et al. (2010).

^j From Olech et al. (1999).

^k From Arellano Ferro et al. (2004).

^l From Clement et al. (1995).

^m From Clement & Shelton (1997).

ⁿ From Arellano Ferro et al. (2006).

^o From Lázaro et al. (2006).

Table 8
Mean Physical Parameters for RRab Stars in Globular Clusters (from Fourier Decomposition)^a

ID	Oo Type	[Fe/H] _{H03}	No. of Stars	[Fe/H] _{ZW84}	[Fe/H] _{J95}	$T_{\text{eff}}^{(V-K)}(\text{K})$	M_V
NGC 6362	I	-0.95	14	-1.26	-0.93	6555	0.86
NGC 6171 (M107)	I	-1.04	3	-1.25	-0.91	6619	0.85
NGC 1851 ^b	I	-1.22	7	-1.43	-1.17	6494	0.80
NGC 5904 (M5)	I	-1.27	26	-1.47	-1.23	6465	0.81
NGC 6266 (M62)	I	-1.29	39	-1.31	-0.99	6501	0.83
NGC 6229	I	-1.43	9	-1.60	-1.41	6383	0.81
NGC 6934	I	-1.54	24	-1.53	-1.31	6455	0.81
NGC 5272 (M3)	I	-1.57	17	-1.60	-1.42	6438	0.78
NGC 7089 (M2)	II	-1.62	9	-1.64	-1.47	6276	0.71
NGC 5286	II	-1.67	12	-1.68	-1.52	6266	0.72
NGC 6809 (M55)	II	-1.81	3	-1.77	-1.65	6333	0.67
NGC 4147	I	-1.83	5	-1.46	-1.22	6633	0.80
NGC 7078 (M15)	II	-2.26	11	-1.92	-1.87	6237	0.67
NGC 6341 (M92)	II	-2.28	5	-1.92	-1.87	6160	0.67

^a References are the same as in Table 7, except as noted.

^b From Kaluzny et al. (2000).

Lyrae stars in M3, based on the temperatures derived by Kaluzny et al. (1998) from their Fourier decomposition of the V -band light curves. Their procedure is essentially identical to the one adopted in our paper to derive the temperatures listed in the last column of Table 6, and thus A -parameter values for M62 RR Lyrae derived on the basis of these temperatures can be directly compared with those for M3 RR Lyrae stars, based on the temperatures derived by Kaluzny and co-workers. As a result, we find for M3 a $\langle A \rangle = 1.803 \pm 0.023$, and for M62 a $\langle A \rangle = 1.806 \pm 0.024$, implying a difference of $\Delta A = 0.003 \pm 0.033$ between M62 and M3. (The standard deviation of the means are indicated.) If due to a difference in He abundance, these values suggest that M62 is more He-rich

than M3, but by only about 0.002 in Y . Within the errors, this comparison suggests that the RR Lyrae stars in M3 and M62 have closely the same He abundance.

On the other hand, the fact that the average A values are closely the same for both M3 and M62 does not necessarily imply that, at any given temperature, no offset between the two clusters in present. To check for the presence of such possible offsets, we compare in Figure 8 the derived distributions. Intriguingly, and in contrast with what was found in Figure 7,⁷

⁷ Recall that the reference OoI line in Figure 7, from Cacciari et al. (2005), indicates the locus occupied by the presumably “unevolved” RR Lyrae stars in M3.

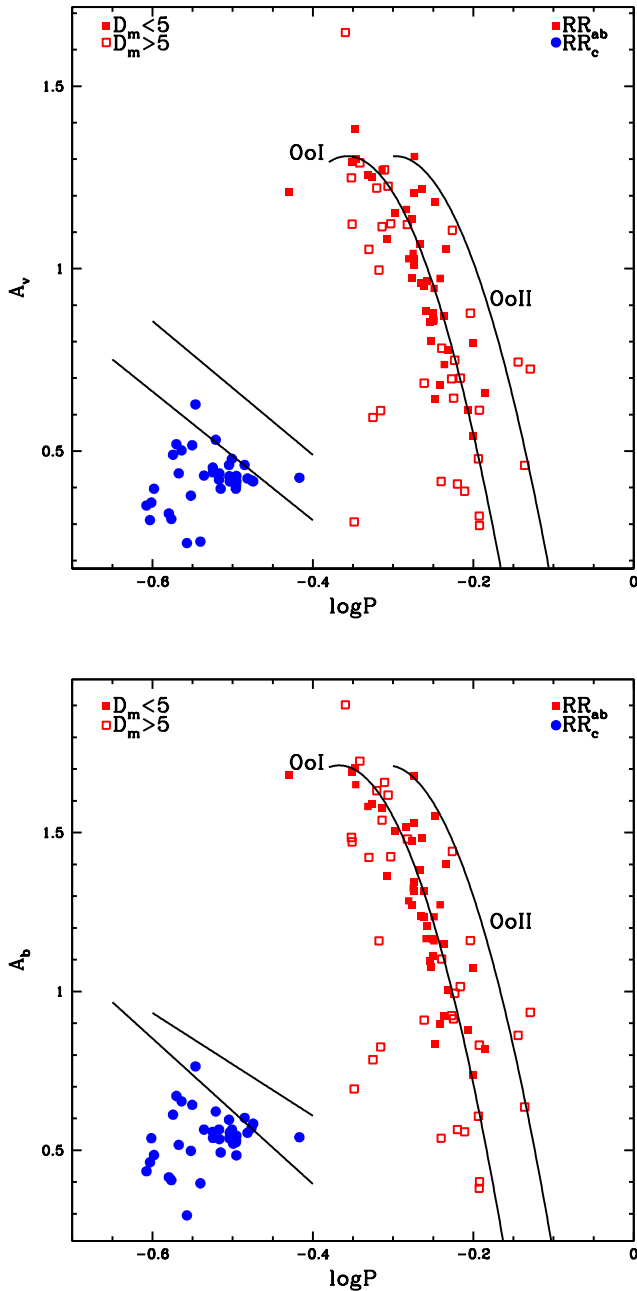


Figure 7. Bailey (period-amplitude) diagram for the RR Lyrae stars in M62, compared with reference lines for RR Lyrae stars in OoI and OoII globular clusters. Top: $A_B - \log P$ diagram; bottom: $A_V - \log P$ plane.

there does appear to be an offset between the two clusters, with the deviation of M62 datapoints from the M3 regression line in the $A - T_{\text{eff}}$ plane (solid line in Fig. 8) amounting to $\Delta A_{T_{\text{eff}}} = 0.020 \pm 0.012$. If due to a difference in He abundance, this would imply that the M62 RR Lyrae stars are more He-rich than their M3 counterparts, by about 0.013 ± 0.008 in Y . This result is confirmed if, instead of the Kaluzny et al. (1998) Fourier parameters for M3 RR Lyrae stars we use those more recently derived by Cacciari et al. (2005). Further work on the temperatures of M62 RR Lyrae stars will be required before we are in a position to conclusively settle this issue.

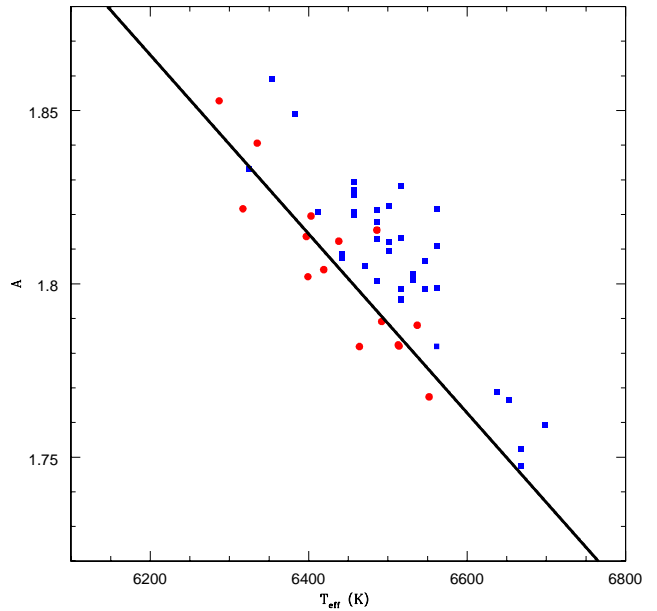


Figure 8. In this figure, A -parameter values, as derived on the basis of equation 3 for ab-type RR Lyrae stars, are plotted as a function of temperature, as derived based on Fourier decomposition ($V-K$ colors). Squares indicate M62 stars, whereas circles represent M3 stars. The straight line is a least-squares fit to the M3 data. See text for more details.

8. SUMMARY

In this paper we have provided a detailed account of the time-series observations that we have collected for the Galactic globular cluster M62, first reported on in Contreras et al. (2005). Our results indicate that M62 is one of the most RR Lyrae-rich (in the sense of total number of RR Lyrae stars present) globular clusters known in the galaxy, and it is actually not unlikely that future studies will reveal that it is *the* most RR Lyrae-rich globular cluster known. In like vein, M62 appears to be the globular cluster with the largest known number of LPV stars in the Milky Way, thus making it a very attractive benchmark object for future RR Lyrae and LPV studies alike.

Discussing the distribution of variable stars in the cluster’s CMD, we find that most of the detected variables are likely cluster members. The CMD of the cluster is, however, severely affected by differential reddening; we have accordingly taken benefit of the large number of RR Lyrae variables that are present in the cluster to build a 2-D reddening map for the cluster, which allowed us to present a “corrected” CMD that is much less strongly affected by differential reddening. A full analysis of the cluster CMD will be presented in a forthcoming paper (Contreras et al. 2010, in preparation).

From an analysis of the pulsation periods of the detected RR Lyrae stars, we provide an updated metallicity $([\text{Fe}/\text{H}]_{\text{ZW84}} = -1.31)$, based on Fourier decomposition of the RR Lyrae light curves) and distance modulus $[(m-M)_V = 15.58]$, based on the recent $M_V(\text{HB}) - [\text{Fe}/\text{H}]$ calibration by Catelan & Cortés 2008] estimates for the cluster. In addition, we discuss a variety of Oosterhoff indicators, including the mean periods, period distribution, and Bailey diagram, and conclude that the cluster is an OoI object, in spite of its blue HB morphology but consistent with its moderately high metallicity. Therefore, metallicity does play an important role in defining Ooster-

hoff type, at least in the case of M62 (see also Contreras et al. 2005). Finally, based on an application of the “A-method,” we conclude that the M62 RR Lyrae stars likely have a similar He abundance as M3, although more work on the temperatures of the M62 RR Lyrae is needed before this result can be conclusively established.

Support for M.C. is provided by MIDEPLAN’s Programa Inicativa Científica Milenio through grant P07-021-F, awarded to The Milky Way Millennium Nucleus; by Proyecto Basal PFB-06/2007; by FONDAP Centro de Astrofísica 15010003; and by Proyecto FONDECYT Regular #1071002. H.A.S. would like to acknowledge the National Science Foundation for support under grants AST0607249 and AST0707756. J.B. acknowledges support from MIDEPLAN’s grant P07-021-F and Proyecto FONDECYT Regular #1080086. We thank an anonymous referee for useful comments that helped improve the presentation of our results.

REFERENCES

- Alard, C. 2000, *A&AS*, 144, 363
 Arellano Ferro, A., Arévalo, M. J., Lázaro, C., Rey, M., Bramich, D. M., & Giridhar, S. 2004, *RevMexAA*, 40, 209
 Arellano Ferro, A., García Lugo, G., & Rosenzweig, P. 2006, *RevMexAA*, 42, 75
 Beccari, G., Ferraro, F. R., Possenti, A., Valenti, E., Origlia, L., & Rood, R. T. 2006, *AJ*, 131, 2551
 Bellazzini, M., Ibata, R., Monaco, L., Martin, N., Irwin, M. J., & Lewis, G. F. 2004, *MNRAS*, 354, 1263
 Blanco, B. M. 1992, *AJ*, 103, 1872
 Bono, G., Caputo, F., & Stellingwerf, R. F. 1995, *ApJS*, 99, 263
 Borissova, J., Catelan, M., & Valchev, T. 2001, *MNRAS*, 324, 77
 Bramich, D. M. 2008, *MNRAS*, 386, L77
 Cacciari, C., Corwin, T. M., & Carney, B. W. 2005, *AJ*, 129, 267
 Caloi, V., Castellani, V., & Piccolo, F. 1987, *A&AS*, 67, 181
 Caputo, F., & Castellani, V. 1975, *Ap&SS*, 38, 39
 Caputo, F., Santolamazza, P., & Marconi, M. 1998, *MNRAS*, 293, 364
 Catelan, M. 2004a, *ApJ*, 600, 409
 Catelan, M. 2004b, in *Variable Stars in the Local Group*, ASP Conf. Ser., 310, ed. D. W. Kurtz & K. R. Pollard (San Francisco: ASP), 113
 Catelan, M. 2007, *RevMexAA Conf. Ser.*, 26, 93
 Catelan, M. 2009, *Ap&SS*, 320, 261
 Catelan, M., & Cortés, C. 2008, *ApJ*, 676, L135
 Catelan, M., & de Freitas Pacheco, J. A. 1993, *AJ*, 106, 1858
 Catelan, M., et al. 2006, *Mem. Soc. Astron. Italiana*, 77, 202
 Clement, C. M., Bezaire, J., & Giguere, D. 1995, *AJ*, 110, 2200
 Clement, C. M., Jankulak, M., & Simon, N. R. 1992, *ApJ*, 395, 192
 Clement, C. M., et al. 2001, *AJ*, 122, 2587
 Clement, C. M., & Shelton, I. 1997, *AJ*, 113, 1711
 Clement, C. M., & Shelton, I. 1999, *ApJ*, 515, L85
 Clementini, G., Corwin, T. M., Carney, B. W., & Sumerel, A. N. 2004, *AJ*, 127, 938
 Clementini, G., et al. 2009, *ApJ*, 704, L103
 Cleveland, W. S. 1979, *J. Amer. Stat. Assoc.*, 74, 829
 Cleveland, W. S., & Devlin, S. J. 1988, *J. Amer. Stat. Assoc.*, 83, 596
 Cocozza, G., Ferraro, F. R., Possenti, A., Beccari, G., Lanzoni, B., Ransom, S., Rood, R. T., & D’Amico, N. 2008, *ApJ*, 679, L105
 Contreras, R., Catelan, M., Smith, H. A., Pritzl, B. J., & Borissova, J. 2005, *ApJ*, 623, L117
 Contreras, R., et al. 2008, *Mem. Soc. Astron. Italiana*, 79, 686
 Corwin, T. M., Catelan, M., Borissova, J., & Smith, H. A. 2004, *A&A*, 421, 667
 Corwin, T. M., Catelan, M., Smith, H. A., Borissova, J., Ferraro, F. R., & Raburn, W. S. 2003, *AJ*, 125, 2543
 Corwin, T. M., Borissova, J., Stetson, P. B., Catelan, M., Smith, H. A., Kurtev, R., & Stephens, A. W. 2008, *AJ*, 135, 1459
 Crane, J. D., Majewski, S. R., Rocha-Pinto, H. J., Frinchaboy, P. M., Skrutskie, M. F., & Law, D. R. 2003, *ApJ*, 594, 119
 D’Antona, F., & Caloi, V. 2008, *MNRAS*, 390, 693
 Deb, S., & Singh, H. P. 2010, *MNRAS*, 402, 691
 Demarque, P., Zinn, R., Lee, Y.-W., & Yi, S. 2000, *AJ*, 119, 1398
 Fiorentino, G., et al. 2010, *ApJ*, 708, 817
 Forbes, D. A., Strader, J., & Brodie, J. P. 2004, *AJ*, 127, 3394
 Gerashchenko, A. N., Kadla, Z. I., & Malakhova, Yu. N. 1997, *IBVS*, 4418, 1
 Harris, W. E. 1996, *AJ*, 112, 1487
 Jurcsik, J. 1995, *AcA*, 45, 653
 Jurcsik, J. 1998, *A&A*, 333, 571
 Jurcsik, J., & Kovács, G. 1996, *A&A*, 312, 111
 Jurcsik, J., & Kovács, G. 1999, *NewA Rev.*, 43, 463
 Kaluzny, J., Hilditch, R. W., Clement, C., & Rucinski, S. M. 1998, *MNRAS*, 296, 347
 Kaluzny, J., Olech, A., & Stanek, K. Z. 2001, *AJ*, 121, 1533
 Kaluzny, J., Olech, A., Thompson, I., Pych, W., Krzeminski, W., & Schwarzenberg-Czerny, A. 2000, *A&AS*, 143, 215
 Kinman, T. D., Saha, A., & Pier, J. R. 2004, *ApJ*, 605, L25
 Kovács, G. 1998, *Mem. Soc. Astron. Italiana*, 69, 49
 Kovács, G., & Jurcsik, J. 1996, *ApJ*, 466, L17
 Kovács, G., & Jurcsik, J. 1997, *A&A*, 322, 218
 Kovács, G., & Kanbur, S. M. 1998, *MNRAS*, 295, 834
 Kovács, G., & Walker, A. R. 1999, *ApJ*, 512, 271
 Kovács, G., & Walker, A. R. 2001, *A&A*, 371, 579
 Kuehn, C., et al. 2008, *ApJ*, 674, L81
 Lafler, J., & Kinman, T. D. 1965, *ApJS*, 11, 216
 Landolt, A. U. 1992, *AJ*, 104, 340
 Lázaro, C., Ferro, A. A., Arévalo, M. J., Bramich, D. M., Giridhar, S., & Poretti, E. 2006, *MNRAS*, 372, 69
 Lee, J.-W., & Carney, B. W. 1999, *AJ*, 118, 1373
 Liller, M. H., & Lichten, S. M. 1978, *AJ*, 83, 41
 Malakhova, Yu. N., Gerashchenko, A. N., & Kadla, Z. I. 1997, *IBVS*, 4457, 1
 Mateu, C., Vivas, A. K., Zinn, R., Miller, L. R., & Abad, C. 2009, *AJ*, 137, 4412
 Mochejska, B. J., Kaluzny, J., Stanek, K. Z., Sasselov, D. D., & Szentgyorgyi, A. H. 2001, *AJ*, 121, 2032
 Moretti, M. I., et al. 2009, *ApJ*, 699, L125
 Morgan, S. M., Wahl, J. N., & Wiecekhorst, R. M. 2007, *MNRAS*, 374, 1421
 Olech, A., Kaluzny, J., Thompson, I. B., Pych, W., Krzeminski, W., & Schwarzenberg-Czerny, A. 1999, *AJ*, 118, 442
 Olech, A., Kaluzny, J., Thompson, I. B., Pych, W., Krzeminski, W., & Schwarzenberg-Czerny, A. 2001, *MNRAS*, 321, 421
 Oosterhoff, P. Th. 1939, *Observatory*, 62, 104
 Oosterhoff, P. Th. 1944, *Bull. Astron. Inst. Neth.*, 10, 55
 Petersen, J. O. 1986, *A&A*, 170, 59
 Piotto, G., et al. 2002, *A&A*, 391, 945
 Pietrinferni, A., Cassisi, S., Salaris, M., & Castelli, F. 2006, *ApJ*, 642, 797
 Possenti, A., D’Amico, N., Manchester, R. N., Camilo, F., Lyne, A. G., Sarkissian, J., & Corongiu, A. 2003, *ApJ*, 599, 475
 Pritzl, B. J., Smith, H. A., Catelan, M., & Sweigart, A. V. 2002, *AJ*, 124, 949; erratum: 2003, *AJ*, 125, 2752
 Pritzl, B. J., Smith, H. A., Stetson, P. B., Catelan, M., Sweigart, A. V., Layden, A. C., & Rich, R. M. 2003, *AJ*, 126, 1381
 Sarajedini, A., Mancone, C. L., Lauer, T. R., Dressler, A., Freedman, W., Trager, S. C., Grillmair, C., & Mighell, K. J. 2009, *AJ*, 138, 184
 Simon, N. R., & Clement, C. M. 1993, *ApJ*, 410, 526
 Simon, N. R., & Teays, T. J. 1982, *ApJ*, 261, 586
 Smith, H. A. 1995, *RR Lyrae Stars* (Cambridge University Press, Cambridge)
 Stellingwerf, R. F. 1978, *ApJ*, 224, 953
 Stellingwerf, R. F., & Donohoe, M. 1987, *ApJ*, 314, 252
 Stetson, P. B. 1987, *PASP*, 99, 191
 Stetson, P. B. 1994, *PASP*, 106, 250
 Suntzeff, N. B., Kinman, T. D., & Kraft, R. P. 1991, *ApJ*, 367, 528
 Sweigart, A. V., & Catelan, M. 1998, *ApJ*, 501, L63
 Tomaney, A. B., & Crotts, A. P. S. 1996, *AJ*, 112, 2872
 Trager, S. C., Djorgovski, S., & King, I. R. 1993, *Structure and Dynamics of Globular Clusters*. ASP Conf. Ser., Vol. 50, ed. S. Djorgovski & G. Meylan (San Francisco: ASP), 347
 Trager, S. C., Djorgovski, S., & King, I. R. 1995, *AJ*, 109, 218; erratum: *AJ*, 109, 218
 van Aagt, S. L. T. J., & Oosterhoff, P. T. 1959, *Ann. Sternw. Leiden*, 21, 253
 van Albada, T. S., & Baker, N. 1971, *ApJ*, 169, 311
 Zinn, R., & West, M. J. 1984, *ApJS*, 55, 45
 Zorotovic, M., Catelan, M., Zoccali, M., Pritzl, B. J., Smith, H. A., Stephens, A. W., Contreras, R., & Escobar, M. E. 2009, *AJ*, 137, 257
 Zorotovic, M., et al. 2010, *AJ*, 139, 357

APPENDIX
SAMPLE LIGHT CURVES

Here we show a representative sample of light curves for the newly discovered variable stars in M62. The full set of derived light curves, including our light curves for the previously known variables in the cluster, can be found in the electronic version of this paper.

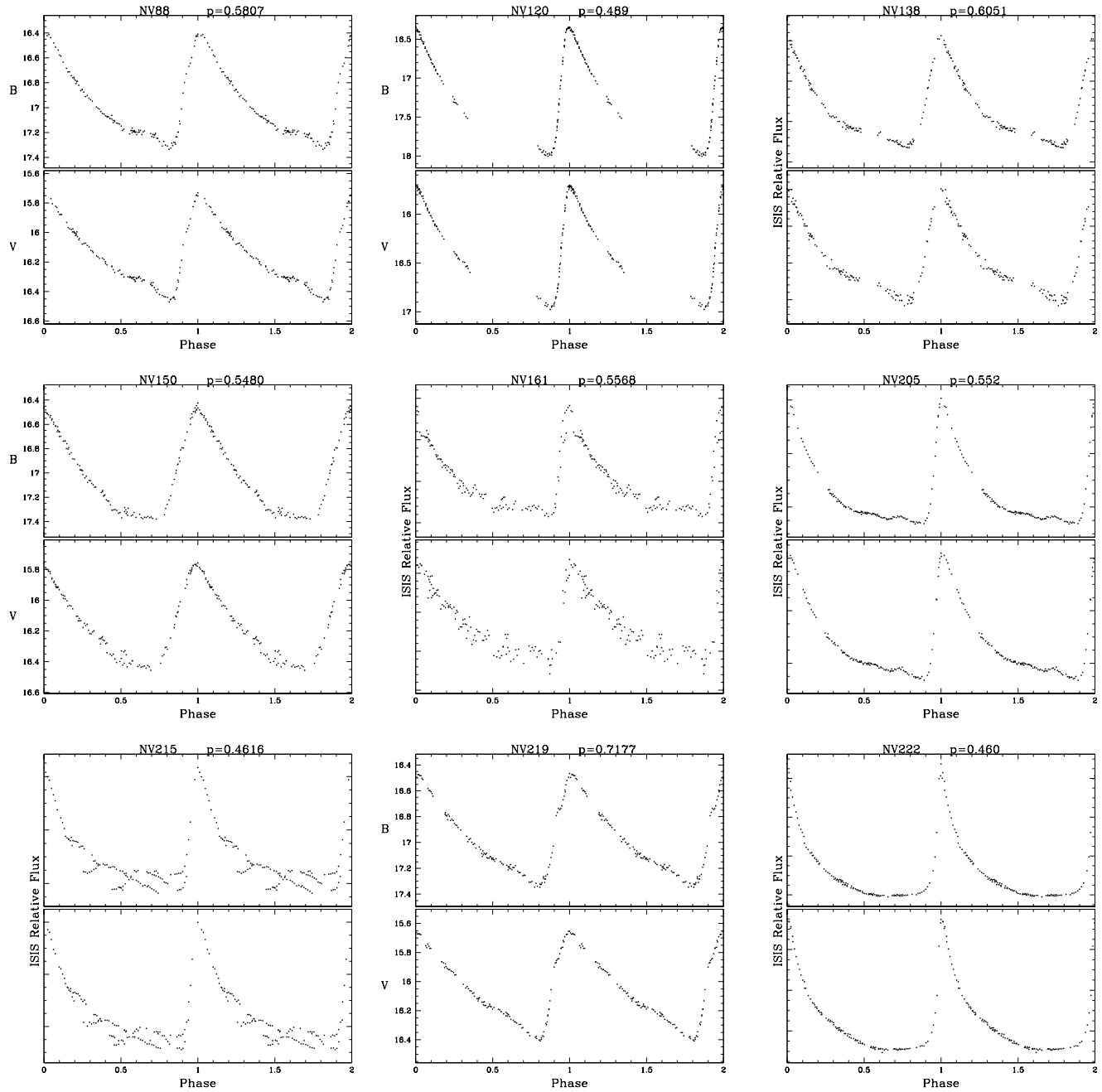


Figure 9. Sample light curves for newly-discovered ab-type RR Lyrae stars. (The full set can be found in the electronic version of this paper.)

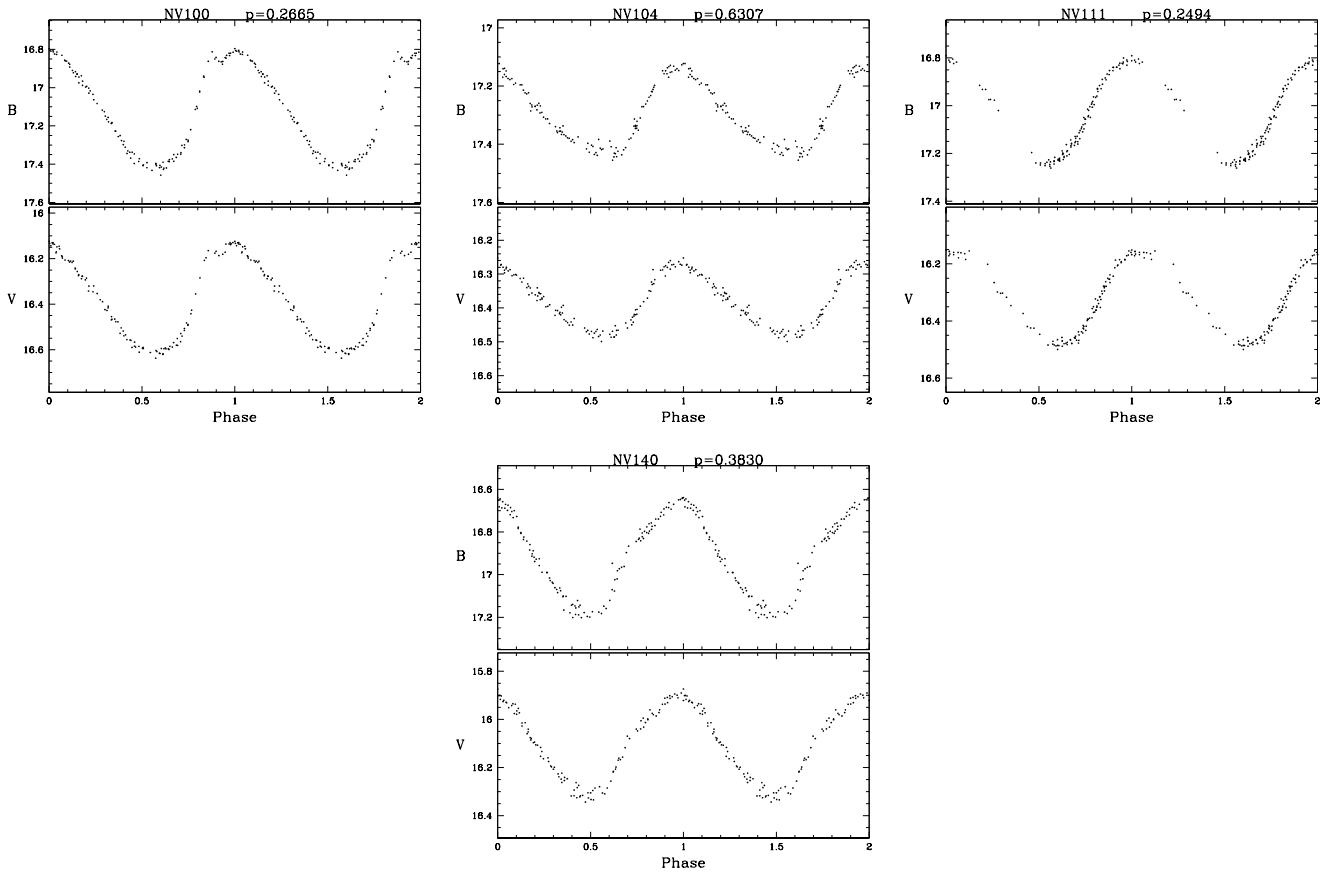


Figure 10. Sample light curves for newly-discovered c-type RR Lyrae stars. (The full set can be found in the electronic version of this paper.)

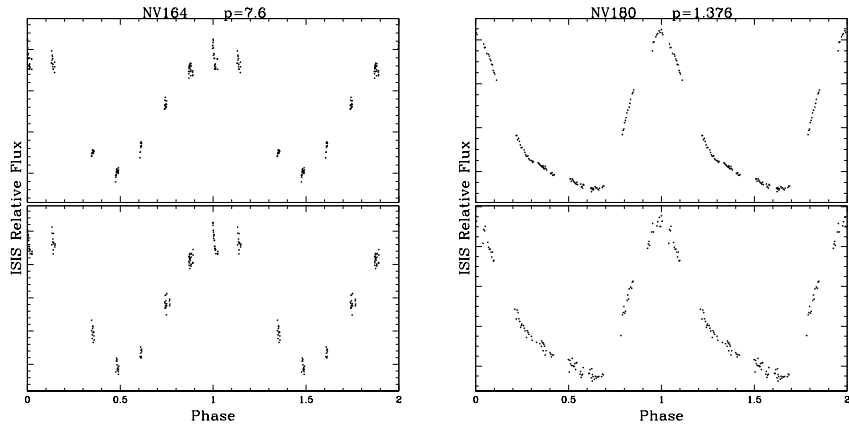


Figure 11. Sample light curves for newly-discovered type II Cepheids. (The full set can be found in the electronic version of this paper.)

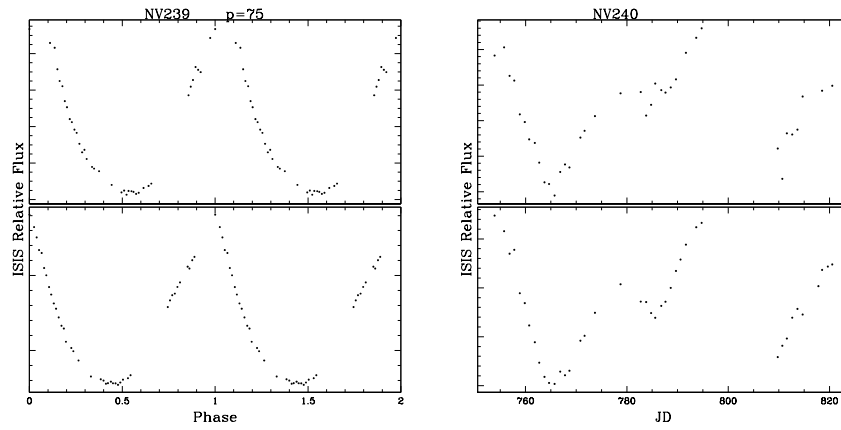


Figure 12. Sample light curves for newly-discovered long-period variables. (The full set can be found in the electronic version of this paper.)

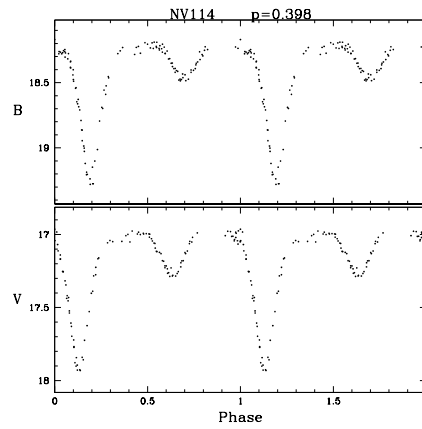


Figure 13. Light curves for NV114, a newly discovered eclipsing binary.

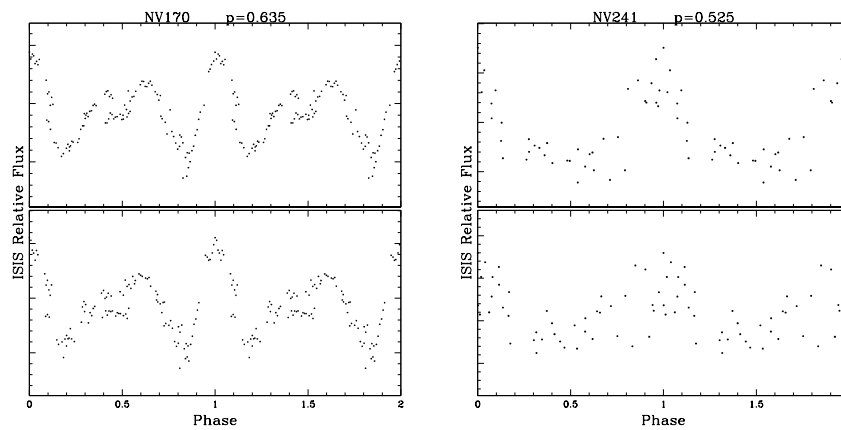


Figure 14. Sample light curves for newly-discovered variable stars whose classification remains unclear. (The full set can be found in the electronic version of this paper.)